ACSNANO

www.acsnano.org

REVIEW

Vision for Ratiometric Nanoprobes: *In Vivo* Noninvasive Visualization and Readout of Physiological Hallmarks

Mohammad Javad Afshari,[#] Xiaju Cheng,[#] Guangxin Duan, Ruixue Duan, Shuwang Wu, Jianfeng Zeng, Zi Gu, and Mingyuan Gao*

Cite This: https://doi.org/10.1021/acsnano.3c01641

Read Online

ACCESS | Metrics & More | Article Recommendations

ABSTRACT: Lesion areas are distinguished from normal tissues surrounding them by distinct physiological characteristics. These features serve as biological hallmarks with which targeted biomedical imaging of the lesion sites can be achieved. Although tremendous efforts have been devoted to providing smart imaging probes with the capability of visualizing the physiological hallmarks at the molecular level, the majority of them are merely able to derive anatomical information from the tissues of interest, and thus are not suitable for taking part in *in vivo* quantification of the biomarkers. Recent advances in chemical construction of advanced ratiometric nanoprobes (RNPs) have enabled a horizon for quantitatively monitoring the biological abnormalities *in vivo*. In contrast to the conventional probes whose dependency of output on single-signal profiles restricts them from taking part in quantitative practices, RNPs are designed to provide information in two channels, affording a self-calibration opportunity to exclude the analyte-independent factors from the outputs and address the issue. Most of the conventional RNPs have encountered several challenges regarding the reliability and sufficiency of the obtained data for high-performance imaging. In this Review, we have summarized the recent progresses in developing highly advanced RNPs with the capabilities of deriving maximized information from the lesion areas of interest as well as adapting themselves to the complex biological systems in order to minimize microenvironmental-induced falsified signals. To provide a better outlook on the current advanced RNPs, nanoprobes based on optical, photoacoustic, and magnetic resonance imaging modalities for visualizing a wide range of analytes such as pH, reactive species, and different derivations of amino acids have been included. Furthermore, the physicochemical properties of the RNPs, the major constituents of the nanosystems and the analyte recognition mechanisms have been introduced. Moreover, the alterations in the values of the ratiometric signal in response to the analyte of interest as well as the time at which the highest value is achieved, have been included for most of RNPs discussed in this Review. Finally, the challenges as well as future perspectives in the field are discussed.

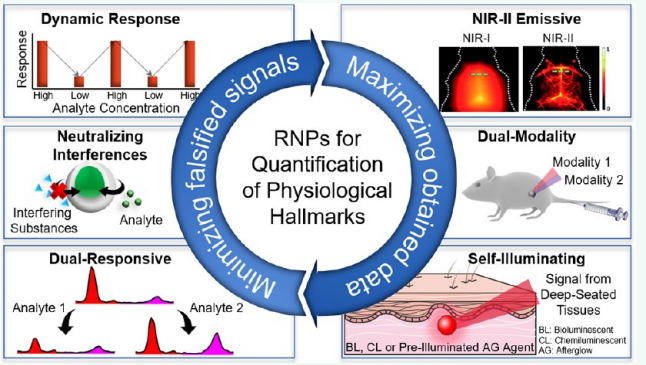

KEYWORDS: *Ratiometric nanoprobes, Quantitative analysis, Noninvasive detection, Disease-associated physiological parameters, Output-disruptive microenvironmental interferences, High-performance imaging, In vivo applications, Optical imaging, Photoacoustic imaging, Magnetic resonance imaging*

1. INTRODUCTION

The incidence of anomalies in the physiological parameters of the human body has been regarded as alarming indications for the emergence of chronic diseases. Those parameters include, but are not limited to, hypoxia, altered extracellular level of reactive species, abnormalities in pH level and irregular variations in the expression or activity of certain proteins and amino acids.[1] For instance, matrix metalloproteinases

Received: February 20, 2023
Accepted: April 3, 2023

(MMPs), which are zinc-dependent secreted endopeptidases with the capability of cleaving peptide bonds of protein molecules into shorter fragments, can be mentioned. This class of enzymes plays critical roles in helping extracellular matrices to maintain and regulate homeostasis as well as a wide range of other physiological processes from cell proliferation to embryonic development.[2] Nevertheless, the pathological involvements of the overexpression of these proteases in inflammation, tumor growth and metastasis, myocardial infarction and heart failure have also been identified.[3] Thus, careful screening of suspicious tissues of patients for their physiological parameters is of great importance, dropping helpful hints about the stage of the diseases, their progression pace and probably the treatment strategies.

Although great efforts have been made to inspect the disease-associated parameters at the molecular level and in *in vitro* practices, the analyzing methods cannot perfectly reflect the correlation of different parameters and their spatiotemporal heterogeneity in the complex biological system of living organisms. As practical alternatives, invasive *in vivo* techniques in which the microenvironment of the suspicious tissue is directly accessed and screened by finely designed electrodes have attracted the attention of medical practitioners. For example, as one of the conventional methods to determine the MMPs activity within the tumor, biopsy treatment has been employed to extract a portion of the tissue for further pathological studies and evaluations.[4] However, due to the lower cell−cell adhesion of tumor cells compared to normal ones, the process of sampling from the tumorous tissues during biopsy might be accompanied by the risk of dislodging a tumor cell that might leak into the bloodstream or interstitial fluid, leading to metastasis.[5] Moreover, since the initially developing tumor tissues consist of miscellaneous and separated cellular subpopulations,[6] the obtained result might be associated with a lack of certainty about the protease distribution in the whole tumor site.[7] Therefore, developing *in vivo* methods that can ensure obtaining detailed and reliable information in a noninvasive manner has aroused great interest.

In recent decades, several well-known noninvasive detecting modalities, including but not limited to optical imaging (OI), photoacoustic (PA) imaging, and magnetic resonance imaging (MRI), have been developed and widely adopted.[8−10] The techniques are operated based on different mechanisms, and each of them has its specific significance as well as seemingly inseparable limitations.[11] Displaying distinctive merits such as high sensitivity and fast feedback as well as several practical mechanisms and decorations for constructing diagnostic agents, optical and photoacoustic imaging techniques have made considerable contributions in the field. On the other hand, although MRI might lag behind OI and PA with regard to the sensitivity of measurements,[12] its undeniable advantages such as the capability of providing information from the deepest organs of human bodies as well as being a well-accepted and relatively ubiquitous clinical technique have encouraged researchers to construct MRI-based diagnostic probes. Regardless of the modality of imaging, engineering the constituents of the probes to overcome the biological barriers hampering the efficient and specific delivery of the probes to the target tissues has attracted considerable attention.[13,14]

Being obsessed with improving the accuracy of measurements and reliability of the obtained data has always been the primary driving force for medical scientists to address the shortcomings of the existing techniques. Therefore, to reduce the background signals arising from the agent molecules that nonspecifically reside in healthy tissues, activatable nanoprobes have been suggested.[15−17] In contrast to the "always on" nanoprobes, the activatable nanoagents are in their "off" mode while nonspecifically captured outside of the microenvironment of interest. Conversly, upon reaching the microenvironment of the target tissue, they would be turned "on", begining to perform the function of interest.[18] Nevertheless, the dependency of the measurements on the intensity of a single signal output which can be easily disrupted by several analyte-independent factors, would undermine confidence in the reliability of the obtained results, posing a major obstacle for the contribution of the corresponding probes in high-precision etiological studies.[19] For instance, the spatiotemporal variation of probe distribution within the tissue of interest, microenvironmental (pH, temperature, *etc.*) influences on the functionality of probes as well as fluctuation in excitation light or instrumental parameters, photobleaching (in cases of optical imaging), the unfavorable interaction of neighboring tissues with the generated signal, and so forth, may all produce false-negative or -positive results.

As one of the practical methods to address the issues, the ratiometric measurement strategies have emerged. Since such measurements are based on dual-signal readout in which one of them is served as the reference and the other as the detecting signal, a self-calibration opportunity can be provided to minimize the influence of the analyte-independent distractions.[20] In contrast to single-intensity based methods, the ratiometric approach can quantitatively scrutinize the alteration in the level of physiological parameters, extending the applicability of the ratiometric probes to *in vivo* investigation of the origin and evolution of chronic diseases. The fast advances in nanomaterials development have enabled state-of-art *in vivo* ratiometric bioimaging of endogenous biological targets such as reactive oxygen species (ROS),[21,22] reactive nitrogen species (RNS),[23−25] reactive sulfur species (RSS),[26−29] derivations of amino acids,[30−33] ions,[34,35] *etc.*[36−38] However, there is still ample room to obtain more satisfactory results from most of these nanosystems either by manipulating the constituents of the probes to improve the imaging performance or minimizing the inevitable interference of environmental factors on the output signal.

Living organisms are characterized by the existence of numerous biological entities and the occurrence of many biological events that might dynamically interact with one another under different environmental parameters such as pH and temperature, either to perform specific functions or as a response to external stimuli. The subtle interplay of the entities, regardless of being advertent or fortuitous, introduces enormous complexities to biological systems, complicating the close *in situ* inspection of a specific biological event of interest. Such complexities necessitate the development of highly advanced nanoprobes to extract sufficient and reliable data from the biological systems in order to accelerate the translation of early diagnosis and individual therapy techniques into widespread clinical practices. Accordingly, developing ratiometric nanoprobes (RNPs) that can somehow be tailored to overcome certain aspects of biological complexities as well as providing maximized information from the biological environments have become the center of attention. In response to the fast development of the field, this Review aims to critically describe the recent progress in constructing such advanced RNPs for *in vivo* quantitative visualization with

https://doi.org/10.1021/acsnano.3c01641
ACS Nano XXXX, XXX, XXX−XXX

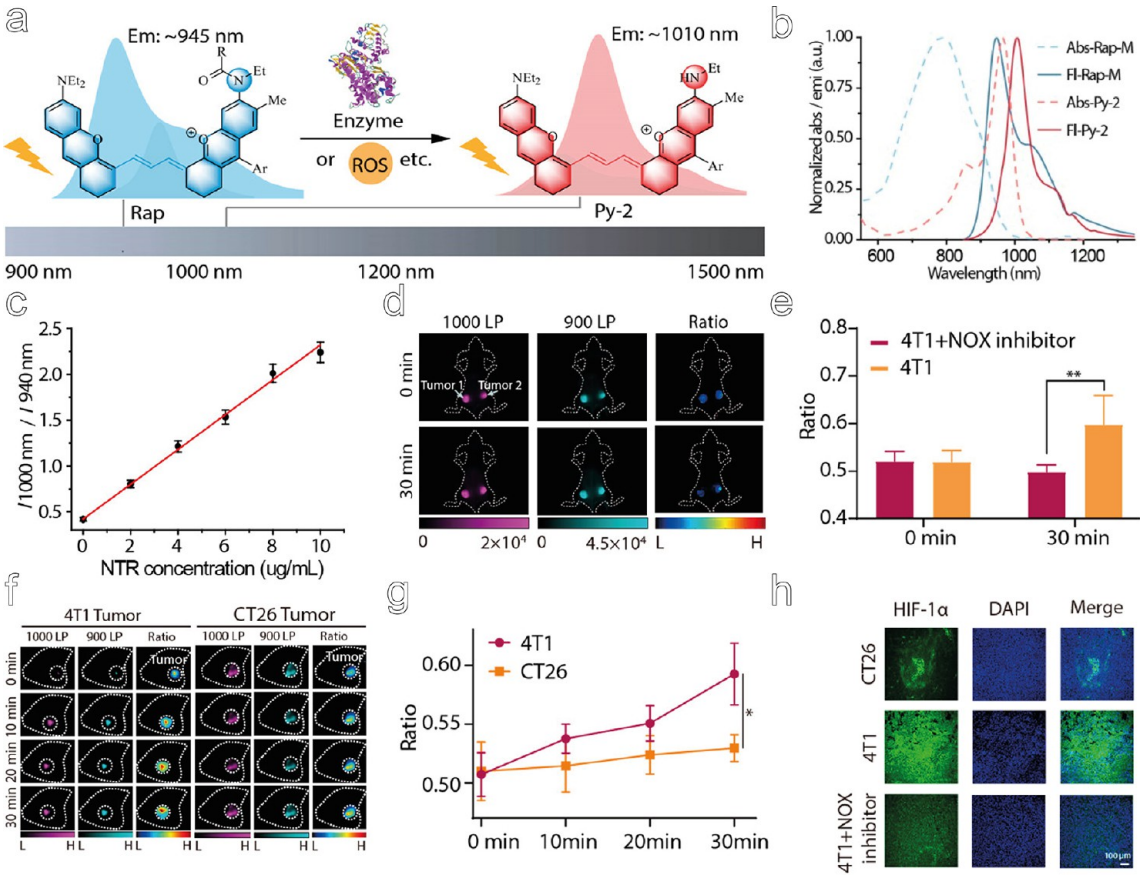

Figure 1. (a) Schematic illustration of probe design and the mechanism of analyte detection. (b) Fluorescence and absorbance intensities of the probes before and after the detection of the analytes. (c) Ratiometric ($F^{ex:808}_{em:1000}/F^{ex:808}_{em:940}$) fluorescence intensities of the probe as a function of the concentrations of nitroreductase. (d) Fluorescence and corresponding ratiometric images of 4T1 tumor-bearing mice. Tumor 1 was pretreated with nitroreductase inhibitor while tumor 2 did not receive any inhibitory agent. (e) The corresponding ratiometric intensities of the experiment represented in frame (d). (f) Fluorescence and corresponding ratiometric images of 4T1 and CT26 tumor-bearing mice models at different time points. (g) The corresponding ratiometric intensities of the experiment represented in the frame (f). (h) Immunofluorescent and DAPI staining of the frozen sections of the primary 4T1 and CT-26 tumors. Adapted with permission from ref. 71. Copyright 2022 American Chemical Society.

several typical paradigms, and the future perspective in the related fields as well.

2. MAXIMIZING OBTAINED DATA FROM BIOLOGICAL MICROENVIRONMENTS

The lack of profound appreciation of biological microenvironments might hinder the development of precise models of the chronic diseases, which in turn impedes the development of highly advanced nanosystems for biomedical applications. For instance, Alzheimer's disease had been primarily diagnosed by certain clinical symptoms (*e.g.*, the memory loss and cognitive decline) until the development of modern imaging techniques revealed that amyloid-β and tau proteins in the brain could serve as the hallmarks of the diseases.[39] Thus, having access to as much information as possible about the microenvironments might be in favor of providing efficient treating strategies for medical conditions at their early stages. This section aims to introduce the recently developed advanced RNPs with the capability of deriving more information from the biological microenvironment, either by providing better spatial resolution *via* employing long-wavelength emissive agents or offering complementary information through integrating multiple imaging modalities.

2.1. NIR-II Emissive RNPs.

The optical- and photoacoustic-based RNPs, which, as mentioned above, afford dual-emission signals, can be roughly categorized into two groups regarding the variation of the signals in respect to one another. Some researchers have designed their systems such that one of the signals remains unchanged during the sensing mechanism, while the other one varies as a direct or indirect response to the analyte of interest. Alternatively, the simultaneous alteration in the intensity of the two signals might also give rise to ratiometric characteristics. The realization of the first approach is usually accomplished by incorporating an analyte-inert agent along with an analyte-sensitive emitting compound into the structure of the probe, in order to provide the reference and measuring signals, respectively. Conversely, molecular structures comprising moieties which are able to recognize the analyte of interest and trigger a disruption in an initial state of charge transfer between the constituents of the system, have formed the foundation of numerous ratiometric probes of the second approach. Förster resonance energy transfer (FRET),[40−43] internal charge transfer (ICT),[25,44−46] excited state intramolecular proton transfer (ESIPT),[47−49] and modulation of π-conjugation pathways[50−52] in the presence of a target have been among the most utilized charge transfer

https://doi.org/10.1021/acsnano.3c01641
ACS Nano XXXX, XXX, XXX−XXX

strategies for achieving ratiometric characteristics with two emission bands.

Currently, it has been widely accepted that the resolution of information obtained through *in vivo* optical and photoacoustic bioimaging, strongly depends on the wavelength values of excitation light and resulting signal.[53,54] In contrast to the values fall into the visible (*ca.*, 400−700 nm) and first near-infrared (NIR-I, *ca.*, 700−900 nm) regions of the electromagnetic wavelength spectrum, the signals of the second near-infrared (NIR-II, *ca.*, 1000−1700 nm) region transmitted within human tissues encounter minimized scattering and absorption.[55] Therefore, although developing NIR-I emissive optical- and photoacoustic-based RNPs is still actively ongoing,[40,41,56−65] constructing NIR-II sensors is more favorable for high-performance *in vivo* imaging from deep-seated organs.

2.1.1. RNPs Based on Organic Materials. The upregulation of intracellular reductases in response to the deficiency of oxygen (O_2) has been exploited as an indirect approach to identifying hypoxic tissues. This class of flavoenzymes, with the help of flavin mononucleotide (FMN) or flavin adenine dinucleotide (FAD) serves as the catalyzer for reduction reaction, comprises several entities such as nitroreductase (NTR), azoreductase, DT-diaphorase, quinone reductase, and cytochrome P450 reductase.[66] Thus far, the majority of fluorescent RNPs for indirect hypoxia mapping have been designed based on NTR-mediated chemical transformation of the probe structure.[67−70] However, Lan *et al.* developed one of the few small molecule-based NIR-II emitting RNPs by constructing a chemical skeleton composed of polymethine and rhodamine 6G dyes as well as the nitrobenzene unit (Figure 1). The intensity of fluorescence (FL) signal arising from the constructed platform (*i.e.*, $F^{ex:808}_{em:940}$, where "ex" and "em" represent excitation and emission wavelengths, respectively) encountered a reduction as the consequent of nitrobenzene cleavage through NTR-mediated 1,6-elimination followed by carbamic acid hydrolysis. Meanwhile, a $F^{ex:808}_{em:1000}$ signal whose intensity was directly proportional to NTR concentration was observed, endowing the prepared probe with ratiometric properties such that the ratiometric signal ($F^{ex:808}_{em:1000}/F^{ex:808}_{em:940}$) was subjected to a 4-fold enhancement in the presence of the analyte (10 μg/mL) in about 45 min. The levels of hypoxia in dicoumarol-treated (NTR-inhibitor) and untreated 4T1 tumor-bearing mice were successfully determined. Moreover, through performing a comparison, the hypoxic level of 4T1 was determined to be significantly higher than that of CT-26 tumors. The high consistencies between the obtained results and the supplementary experiments (*e.g.*, immunofluorescent staining) as well as the predicted results from the literature confirmed the reliability of the proposed nanoprobe. In addition, substituting nitrobenzene with benzyl boronate, the practicality of the strategy to be expanded to ROS quantification in mice suffering from drug-induced liver injury was also verified.[71] However, since benzyl boronate has been also utilized as a well-known recognition unit for RNS,[72−74] this derivative of the probe might not be able to take part in applications in which ROS and RNS need to be distinguished from one another.

Albumin is one of the most critical and abundant liver-produced proteins that plays a diverse range of pathological roles. Many studies have shown that serum albumin tends to decrease in patients suffering from cancer.[75] This state of albumin deficiency (hypoalbuminemia) might be the consequent of several causes including inflammation and other physiological stresses within the tumor as well as an elevated rate of lysosome-mediated albumin catabolism in cancer cells as a way to provide the necessary energy needed for their accelerated growth.[76] Hence, surveying the albumin level can provide valuable information about the severity, progression, and prognosis of numerous cancers. The lack of alkylation on the nitrogen atom of their indolenine heterocycles prevents norcyanines dyes from the formation of the cationic "cyanine-like" state with high absorption coefficient in long wavelengths, unless in the media with reduced pH.[77] Moreover, the dyes exhibit a pH-responsive fluorescence emission that has been attributed to the reversible equilibrium between the protonated and deprotonated forms of their structures. Usama *et al.* showed that a more extensively delocalized structure can be achieved by replacing indolenine heterocycles with benzo-[c,d]indoles capable of being converted to a nonalkylated norcyanines form, resulting in a bathochromic shifted chromophore with an extension in its absorbance spectrum toward the NIR-II region upon protonation. The shift in the absorption profile in response to pH afforded the ratiometric characteristic such that the emission spectra under two different excitation wavelengths (*i.e.*, $F^{ex:1064}_{em:1275}$ and $F^{ex:785}_{em:1275}$) exhibited antagonistic trends. It was shown that the constructed pH-responsive molecular scaffold could effectively and quantitatively detect the albumin lysosomal uptake in living mice bearing JIMT-1 breast cancer xenografts. Upon intratumoral administration of the probe, the $F^{ex:1064}_{em:1275}/F^{ex:785}_{em:1275}$ signal increased from 0 to 0.87 ± 0.08 within 96 h postinjection.[78]

2.1.2. RNPs Based on Inorganic and Hybrid Materials. Apart from a few reported RNPs based on small molecules, the majority of NIR-II emissive RNPs have been developed by employing quantum dots (QDs)[79−81] and down conversion nanoparticles (DCNPs).[82−86] Lanthanide (Ln)-doped DCNPs have attracted great interest due to their large Stokes shifts, photostabilities, narrow emission profiles, and long fluorescence lifetimes. By codoping trivalent lanthanide cations as activators (*e.g.*, Er^{3+}, Nd^{3+}, Ho^{3+}, Pr^{3+} and Tm^{3+}) and sensitizers (*e.g.*, Nd^{3+} and Yb^{3+}) into suitable host matrixes (*e.g.*, $NaYF_4$, $NaGdF_4$ and $LiYF_4$), the emission of DCNPs can be tuned to fall into the entire NIR-II window, based on the application of interest.[87] The insensitivity of the signals of QDs and Ln-doped DCNPs to most of the biological entities has made these nanoparticles suitable candidates for serving as the reference signal in a great deal of NIR-II emissive RNPs. Thus, the nanoprobes are designed by employing either of the nanoparticles along with another fluorescent agent whose emission profile can undergo a fluctuation by certain mechanisms in the presence of an analyte.[82−84,88−95]

For instance, to construct a DCNP-based sensor for visualizing rheumatoid arthritis (RA)-induced inflammatory response, Sun *et al.* finely optimized Nd^{3+} dopant concentration as well as thickness of passivation (P) and buffer layers (B) of DCNPs with the aim of manipulating the energy migration pathways. As a result, a NIR-II emissive hydrophilic probe ($NaErF_4$@B@$NaYF_4$:10%Nd@P) possessing a dual-emission property under a single wavelength excitation ($F^{ex:808}_{em:1060}$ and $F^{ex:808}_{em:1525}$) was achieved. Moreover, the RNS-responsive A1094 dye with a strong absorption at the NIR-I region was conjugated on the surface of DCNPs to serve as a quencher for $F^{ex:808}_{em:1060}$ through the inner filtration (IF) effect. In the presence of the species, however, a reduction in FRET

https://doi.org/10.1021/acsnano.3c01641
ACS Nano XXXX, XXX, XXX−XXX

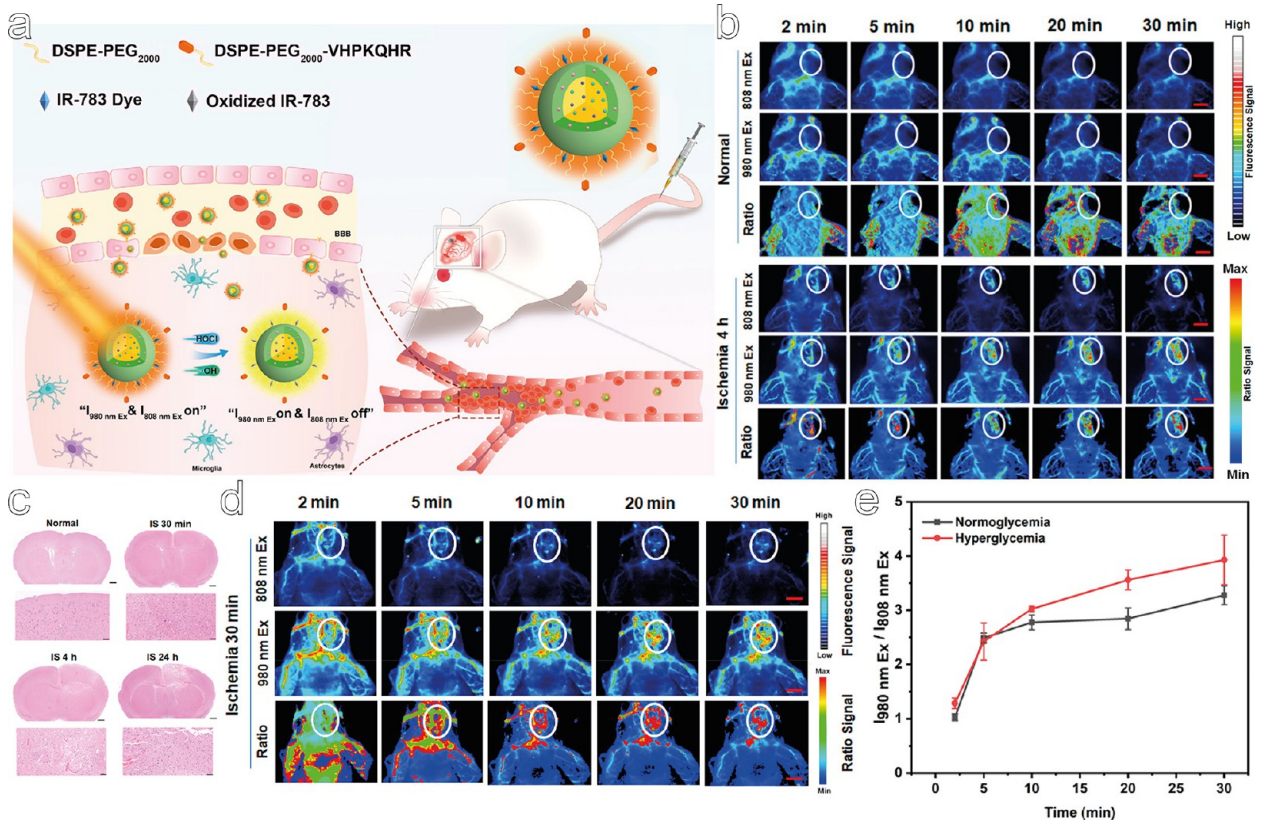

Figure 2. (a) Schematic illustration of probe design and the mechanism of ratiometric detection of HCIO and •OH. (b) $F^{ex:808}_{em:1550}$, $F^{ex:980}_{em:1550}$, and ratiometric ($F^{ex:980}_{em:1550}/F^{ex:808}_{em:1550}$) fluorescence images of normal mice and those with cerebral ischemia modeled for 4 h, at different time points. (c) H&E staining for normal brain and ischemic lesion tissues modeled for different time points. (d) Fluorescence and ratiometric images of hyperglycemia mice with cerebral ischemia modeled for 30 min, at different time points. (e) The corresponding ratiometric intensities of the experiment represented in frame (d). Scale bars in frame (b) and (d) represent 2.5 mm. Adapted with permission from ref. 86. Copyright 2021 American Chemical Society.

efficiency occurred that eliminated the IF effect and revived $F^{ex:808}_{em:1060}$, while $F^{ex:808}_{em:1525}$ remained unchanged. Exhibiting great consistency with X-ray detection and H&E staining, the ratiometric signal arising after the injection of the probe into the joint cavity of RA mice models encountered a 2.65-fold enhancement within 30 min. It was shown that the signal could accurately determine the concentration of peroxynitrite ($ONOO^-$) in the area.[82]

The indistinct and complex features highlighting the onsets of drug-induced liver injury (DILI) have made it difficult to be diagnosed at an early stage, putting it among one of the top leading causes of death worldwide.[96,97] It has been suggested that the overexpression of nitric oxide (NO) in the liver might disrupt several biofunctions of the organ such as the metabolizing lipids and glucose and synthesizing proteins, inducing liver damage.[98,99] Therefore, quantifying assessment of NO level has been suggested as a feasible method for early detection of DILI.[100,101] To develop such a sensor, Bai *et al.* conjugated electron-withdrawing cyanine dyes ($F^{ex:808}_{em:1050}$) with an electron-donating o-phenylenediamine group in order to quench the fluorescence intensity of the dye through an intramolecular photoinduced electron transfer (PET) mechanism. The prepared molecule, which due to the existence of o-phenylenediamine linker was rendered NO-sensitive,[85,102−104] was embedded into mesoporous SiO_2 carriers along with NO-inert $NaYF_4$:Yb/Er DCNPs ($F^{ex:980}_{em:1550}$). The NO-induced transformation of o-phenylenediamine into weak electron-donating and hydrolyzable benzotriazole intermediates obstructed the PET process, leading to the revival of $F^{ex:808}_{em:1050}$ as the detecting signal. Particularly, the $F^{ex:808}_{em:1050}/F^{ex:980}_{em:1550}$ signal reached to 2.4 times of its initial value within 90 min postinjection of the probe into BALB/c nude mice suffering from acetaminophen (APAP)-induced DILI. Monitoring the signal arising from the liver of the animals, the *in vivo* overexpression as well as the suppression of the NO level during APAP-induced DILI and the subsequent APAP antidote treatment, respectively, were identified.[85]

An elevated level of oxidative stress, especially induced by highly reactive oxygen species (HROS) such as HCIO and the hydroxyl radical (•OH), is shown to be associated with the onset, progression, and the severity of a cerebral ischemic stroke (IS), which in turn triggers a series of pathological conditions. The pathological changes might eventually lead to blood clotting, neurologic impairment, and irreversible damage to the brain tissue.[105] Therefore, to develop RNPs for timely assessing IS, IR-783 dye, whose emission profile perfectly overlapped with the absorption band of Nd^{3+} in Ln-doped DCNPs ($NaYbF_4$:5%Er,5%Ce@$NaYF_4$:20%Nd), was employed (Figure 2). The polymethine chain of the dye was prone to undergo one-electron oxidization and cleavage in the presence of HROS, endowing the fluorophore with the dual-role of HROS-targeting site and sensitizer for the prepared Ln-doped DCNPs. Decorating the system with the vascular cell adhesion molecule-1 (VCAM-1)-sensitive peptide facilitated targeting the impaired blood−brain barrier (BBB) as well as activated brain endothelial cells in the ischemic area of mice,

https://doi.org/10.1021/acsnano.3c01641
ACS Nano XXXX, XXX, XXX−XXX

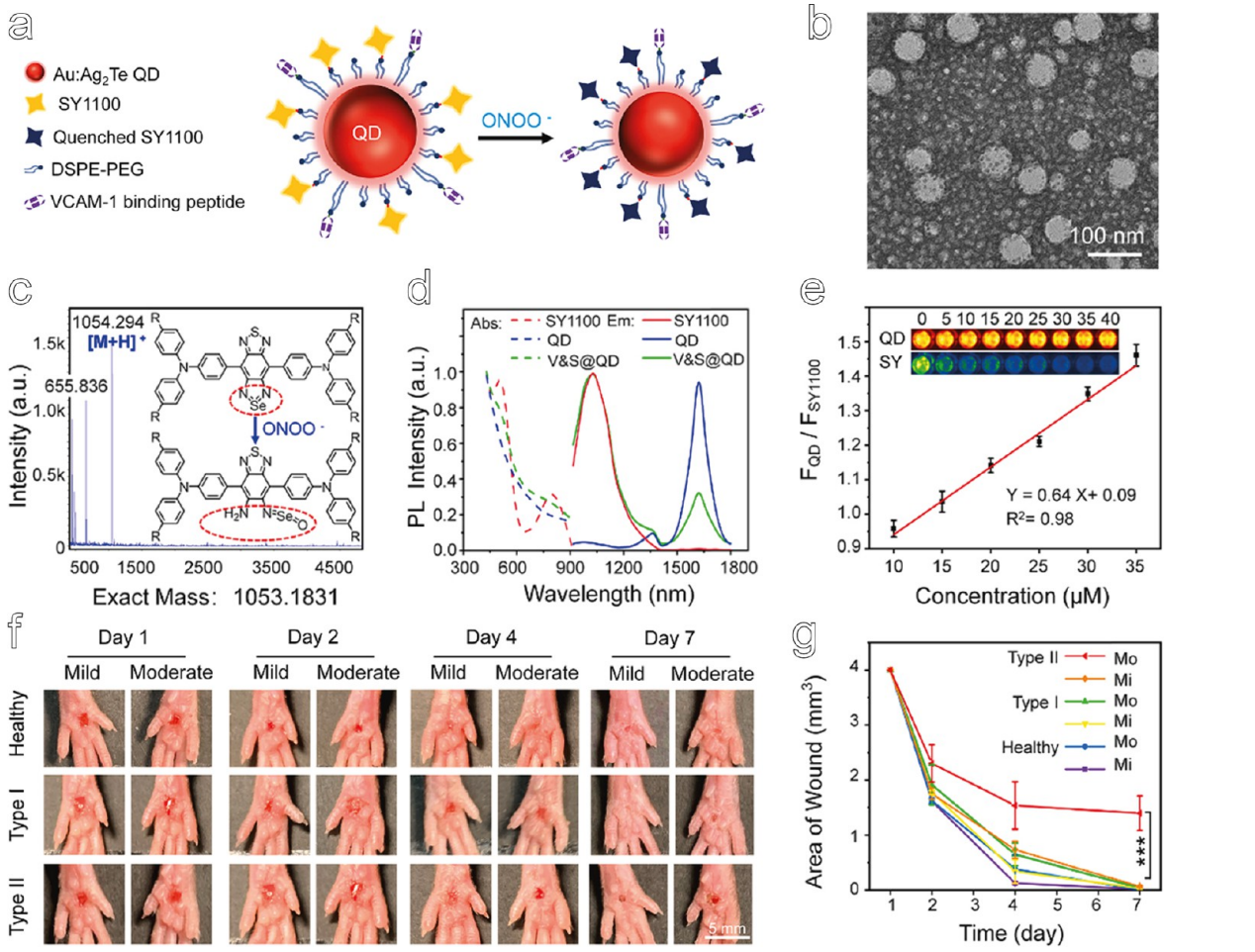

Figure 3. (a) Schematic illustration of probe design and the mechanism of peroxynitrite detection. (b) TEM image of the prepared probe. (c) Recognition mechanism of peroxynitrite by SY1100 molecules (R = CH_2CH_2COOH). (d) Fluorescence and absorbance intensities of the constituents of the probe during different stages of preparation. (e) Ratiometric ($F^{ex:808}_{em:1600}/F^{ex:508}_{em:1025}$) fluorescence intensities of the probe versus different concentrations of peroxynitrite. (f) The wound healing progression in forefeet of normal, type I, and type II diabetic mice models. (g) The corresponding plot of wound healing progression of the experiment represented in frame (f). Adapted with permission from ref. 80. Copyright 2022 Elsevier.

where the presence of HROS suppressed the sensitization process. The process distinctly diminished the intensity of $F^{ex:808}_{em:1550}$ while that of $F^{ex:980}_{em:1550}$ did not change. The authors could identify the correlation between the severity of the condition and the level of oxidative stress and also detect the lesion site of an IS in its early stages, which was not discernible by MRI. Moreover, the salvageable and infarcted areas in the lesion site could be discriminated and the aggravation effect of high blood sugar (hyperglycemia) on oxidative stress as well as the subsequent IS-induced brain damage were identified, evidenced by a 1.2-fold enhancement in the $F^{ex:980}_{em:1550}/F^{ex:808}_{em:1550}$ signal.[86]

Monitoring the healing stages of diabetic wounds helps biomedical engineers to come up with more efficient strategies to accelerate the healing process. Since the oxidative/nitrosative stress and the consequent induction of inflammatory responses have been observed in the wound area, scrutinizing the level of ROS and RNS has been suggested to be a feasible method to pursue the goal.[106,107] To provide RNPs for grading diabetic ischemic/reperfusion injuries, Au:Ag_2Te QDs ($F^{ex:808}_{em:1600}$) as the $ONOO^-$-inert agents were coated with $ONOO^-$-sensitive SY1100 dye molecules ($F^{ex:508}_{em:1025}$) and the VCAM-1 peptide (Figure 3). Since chalcogenides are prone to undergo a reaction with oxidative and nitrosative species,[21,80,108−110] the reaction between the analyte and selenium element in SY1100 perturbed the electron transfer within the dye and quenched the $F^{ex:508}_{em:1025}$ signal. The probe could successfully target the lesion areas of diabetic mice and determine the relationship between the level of $ONOO^-$ and the progression of foot ulcers in both type I and II diabetic models as a manner to predict the healing response. Particularly, it was shown that the intensity of $F^{ex:808}_{em:1600}/F^{ex:508}_{em:1025}$ signals arising from moderate injuries of type I and type II diabetic mice were respectively ∼1.2 and ∼1.8 times higher than those of healthy models.[80]

It can be inferred that analyte-sensitive dyes can be matched well with the NIR-II emissive nanoparticles to achieve a higher contrast between the states of absence and presence of the analyte, offering higher values of the signal-to-noise ratio. As mentioned above, NIR-II RNPs constructed based on the strategy incorporate dye molecules as one of the main constituents of the probe decoration. This might render the synthesis process intricate due to the necessity of performing robust optimizations to minimize the cytotoxicity and self-quenching effects of the molecules. However, since the current well-known photostable and biocompatible NIR-II emissive

https://doi.org/10.1021/acsnano.3c01641
ACS Nano XXXX, XXX, XXX−XXX

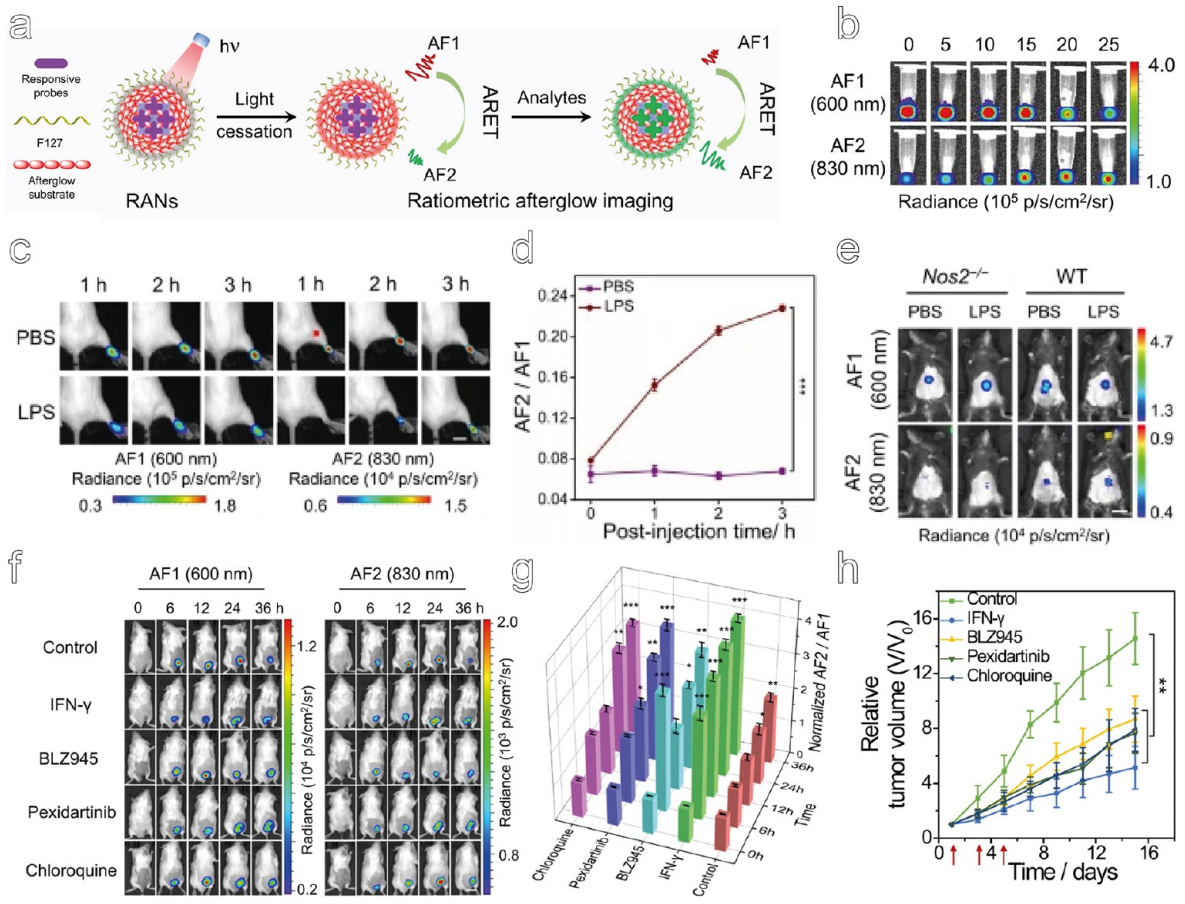

Figure 4. (a) Schematic illustration of the probe constituents and the mechanism of ratiometric visualization. (b) Afterglow images of probe solution upon addition of different concentrations of NO (0−25 μM) (c) Afterglow images of mice pretreated with PBS or LPS at different time points postinjection of the probe. Scale bar represents 1 cm. (d) The corresponding ratiometric ($A_{em:830}/A_{em:600}$) intensities of the experiment represented in frame (c). (e) Afterglow images of mice with the *Nos2* gene knocked out (*Nos2*−/−) and wild type (WT) mice upon intravenous injection of the probe in the LPS-induced liver injury model. (f) Afterglow images of 4T1 tumor-bearing mice pretreated with different kinds of modulators followed by intravenous injection of the probe. Scale bars in frame (e) and (f) represent 2 cm. (g) The corresponding quantification of afterglow intensity ratios of the experiment represented in frame (f). (h) Changes in tumor volume of mice treated with different modulators versus time. Adapted with permission under a Creative Commons CC BY License from ref. 120. Copyright 2022 Springer Nature.

nanoparticles lack the sensitivity toward the alteration in the level of biological entities, the advantages of utilizing analyte-sensitive dyes in the decoration outweigh its disadvantages.

As a feasible technique to provide "dye-free" NIR-II emissive RNPs, Ag nanodots were deposited on the surface of the $F^{ex:1525}_{em:980}$ emissive Ln-doped DCNPs ($NaYF_4$:Gd/Yb/Er@$NaYF_4$:Yb@SiO_2), resulting in a nano myrica rubra-like structure. Taking part in an *in situ* sulfuration reaction with the hydrogen sulfide (H_2S) species in the environment, Ag_2S QDs with the emission of $F^{ex:808}_{em:1053}$ could be produced on the surface of the structure. The probe was designed to quantify the level of metformin, a well-known medicine prescribed for treating a vast range of disorders including type-2 diabetes,[111] cardiovascular diseases, cancer, COVID-19, *etc.*[112] The medicine, however, can trigger a series of side effects such as hepatotoxicity, stomachache, and heartburn.[113] The hepatotoxicity effect of metformin is strongly and dose-dependently correlated with the overexpression of H_2S in the liver tissue upon taking a high dosage of the medicine. The emerging $F^{ex:808}_{em:1053}$ signal whose intensity exhibited a S^{2-} concentration dependent tendency, allowed the probe to sensitively and ratiometrically inspect hepatocytes state for S^{2-} as the early biomarker of metformin-induced hepatotoxicity in living mice treated with the drug. A 3.2-fold enhancement in the $F^{ex:808}_{em:1053}/F^{ex:980}_{em:1525}$ signal was observed within 48 h after metformin administration to mice models. The degree of liver injury predicted by the *in vivo* results was in great consistency with those derived from blood biochemical analyses (*i.e.*, aspartate aminotransferase and alanine aminotransferase) as well as the *ex vivo* determined S^{2-} concentration and cystathionine-γ-lyase (CSE) expression level.[81]

2.2. Self-Illuminating RNPs. The superiorities of self-illuminating imaging techniques such as bioluminescence, chemiluminescence, and afterglow over fluorescence imaging in terms of providing a higher signal-to-noise ratio and potentially visualizing deep-seated organs have been well investigated during the past decade.[114−116] Consequently, employing the excitation-free signals as one of the detecting signals of RNPs has offered the researcher the opportunity to provide maximized and less distorted information from the tissues of interest.[117−121]

Real-time quantification of O_2 and singlet oxygen ($^1O_2$) levels is of great importance for monitoring photodynamic therapy (PDT) efficiency, necessitating powerful platforms to

https://doi.org/10.1021/acsnano.3c01641
ACS Nano XXXX, XXX, XXX−XXX

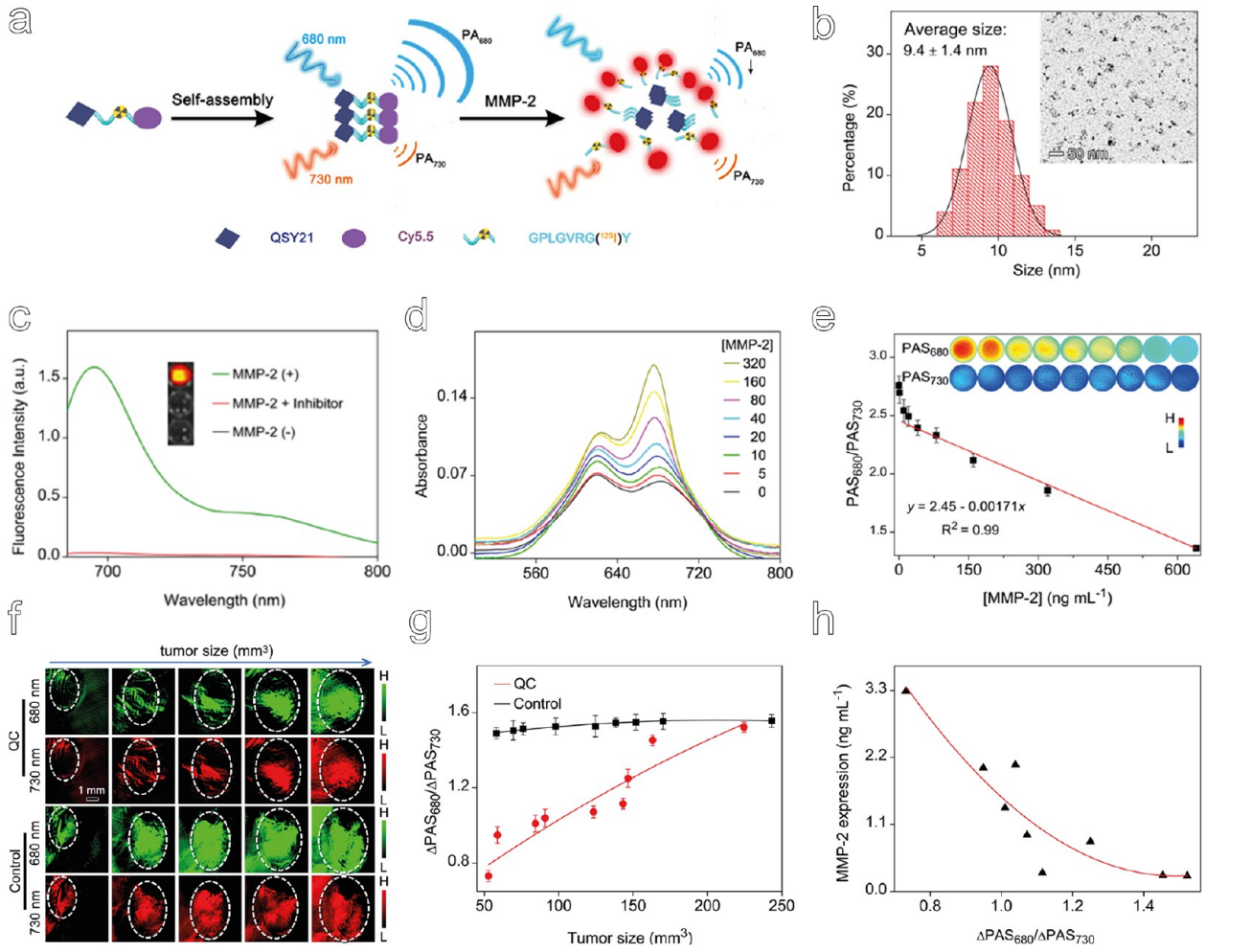

Figure 5. (a) Schematic illustration of probe design and the mechanism of ratiometric photoacoustic visualization of MMP-2. (b) Size distribution of the probe. Inset: corresponding TEM image. The scale bar represents 50 nm. (c) Variation of fluorescence intensity in response to 2 h incubation of the probe with MMP-2 and its inhibitor. Inset: corresponding fluorescence images upon 675 nm laser excitation. (d) Absorbance spectra recorded following incubation of the probe with different concentrations of the analyte. The concentrations are represented in ng/mL. (e) Ratiometric (PA_{680}/PA_{730}) photoacoustic intensities of the probe versus different concentrations of MMP-2 after 2 h of incubation. Inset: PA images of samples containing the probe and different concentration of the analyte. (f) PA images of differently sized 4T1 tumors recorded in 680 and 730 nm channels at a time point equals 2 h postinjection of the probe (QC) and its control. (g) Variation of ratiometric signals generated by the probe and its control, versus the size of the tumor. (h) Quantified expression level of the enzyme through ratiometric photoacoustic imaging. Adapted with permission from ref. 1. Copyright 2019 American Chemical Society.

overcome some challenges such as low detection sensitivity and autofluorescence interference.[122] To develop such nanosystems, photosensitizer Chlorin e6 (Ce6) and a thiophene-based small molecule (2SeFT-PEG) were encapsulated into a micelle by employing DSPE-PEG. Upon production of $^1O_2$ by irradiating Ce6 under 660 nm energy excitation, the thiophene group was oxidized to generate a chemiluminescence signal (C_{1050}). However, the oxidation-mediated destructions in the structure of 2SeFT-PEG induced a noticeable reduction in the fluorescence intensity ($F_{em:1050}^{ex:808}$) of the molecule. Thus, analyzing the ratio of chemiluminescence to fluorescence signals provided a feasible strategy for *in vivo* inspection of O_2 consumption and $^1O_2$ production during the course of PDT. Upon 660 nm laser-pulse irradiation of a tumor site, the ratio increased from 0.38 ± 0.03 to 2.38 ± 0.04 within 15 min of irradiation, indicating that the continuous laser irradiation could generate about 71 ± 10.2 μM of $^1O_2$ (calculated by a previously obtained standard curve) in the region. Although the biochemical indicators in the blood samples of the treated mice showed no abnormalities, the inverse proportionality between the ratiometric signal and the tumor volume as well as caspase-3 concentration were identified during the therapy, enabling the probe to take part in the early evaluation of the PDT. In addition, by inspecting blood oxygen saturation in a tumor, the optimal time interval between the sessions of PDT as well as the laser irradiation time of each session were achieved.[118]

Depending on the microenvironment stimuli, macrophages, as one of the most important immune cells, are able to be differentiated into specific phenotypes to perform certain biological functions in a process referred to as macrophage polarization.[123] With respect to their activation states and functions, macrophages are generally classified into M1 and M2. The former is activated by lipopolysaccharide (LPS) and Th1 cytokines (such as IFN-γ and TNF-α) and metabolizes arginine into citrulline and NO, taking part in microbicidal and

https://doi.org/10.1021/acsnano.3c01641
ACS Nano XXXX, XXX, XXX−XXX

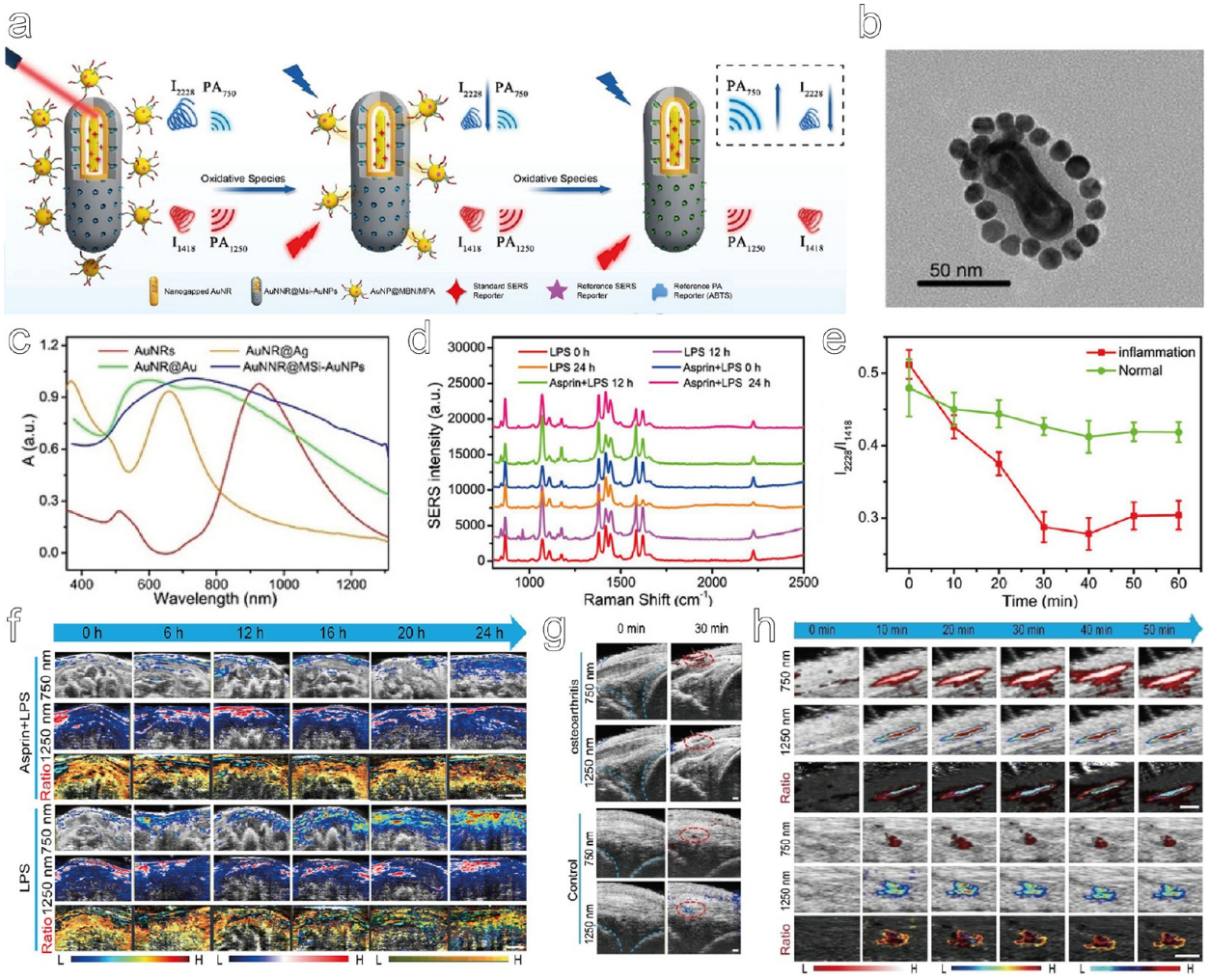

Figure 6. (a) Schematic illustration of the structure of core−satellite RNPs and the mechanism of dual-ratiometric photoacoustic and SERS modalities for visualizing oxidative species. (b) SEM image of the prepared nanostructure. (c) Absorbance spectra of the prepared RNPs during different stages of preparation. (d) SERS spectra of LPS-induced inflammation and anti-inflammatory groups of mice models at different time points after treatment. (e) Ratiometric SERS intensity in normal and LPS-induced peritonitis models. (f) PA_{750} and PA_{1250} and ratiometric (PA_{750}/PA_{1250}) photoacoustic imaging of the LPS-induced inflammation and the anti-inflammatory groups at 30 min postinjection in mice models. Scale bar represents 5 mm. (g) Ultrasound images of knee osteoarthritis performed by PA_{750} and PA_{1250} signals at 0 and 30 min postinjection in rabbit models. The articular cavity and photoacoustic signals are indicated with dashed blue and red circles, respectively. (h) PA_{750} and PA_{1250}, and ratiometric PA_{750}/PA_{1250} photoacoustic imaging of knee affected by osteoarthritis (the upper three rows) and normal knee (the lower three rows) of the rabbit models. Scale bars in frame (g) and (h) represent 1 mm. Adapted with permission from ref. 131. Copyright 2021 John Wiley and Sons.

tumoricidal responses. On the other hand, M2 is alternatively activated by IL-4 or IL-10 and produces ornithine and urea from arginine, serving an anti-inflammatory function.[124] As one of the most promising strategies in immuno-oncology, targeting the tumor-associated macrophages (TAMs) that are heavily populated in the solid tumors microenvironment has attracted enormous interest.[125] In this strategy, TAMs are modulated to be polarized into an antitumorigenic M1 phenotype. Thus, quantitative monitoring of biomarkers such as NO can serve as a representation for the polarization of TAMs into M1, making it of paramount importance, which sheds more light on the interaction between the immune system and cancer cells in macrophage-modulated immunotherapy.[126,127] Imitating the FRET mechanism and employing self-assembly chemistry, poly[2methoxy-5-(2-ethylhexyloxy)-1,4-phenylenevinylene] (MEHPPV)) as the afterglow substrate and the energy donor was brought in close proximity to a NO-responsive fluorophore acceptor to realize the "afterglow resonance energy transfer" (ARET) between the donor and acceptor. In the presence of NO and as a consequence of ICT occurrence, the initial acceptor molecule was oxidized to form 5H[1,2,3]triazolo[4,5-*f*]-2,1,3-benzothiadiazole with an improved energy accepting capability (Figure 4). Upon irradiation cessation and the consequent $^1O_2$ generation by afterglow initiators, the stored energy in the unstable intermediate could be radiatively released ($A_{em:600}$) or nonradiatively transferred to the activatable acceptor through ARET, initiating another afterglow with a red-shifted emission ($A_{em:830}$). Thus, the two resulting afterglow emissions enabled the probe to achieve ratiometric properties. The probe was employed to evaluate the anticancer effectiveness of four different macrophage polarization modulators, namely, interferon-γ (IFN-γ), BLZ945, pexidartinib, and chloroquine for tumor immunotherapy in 4T1 tumor-bearing mice. The

https://doi.org/10.1021/acsnano.3c01641
ACS Nano XXXX, XXX, XXX−XXX

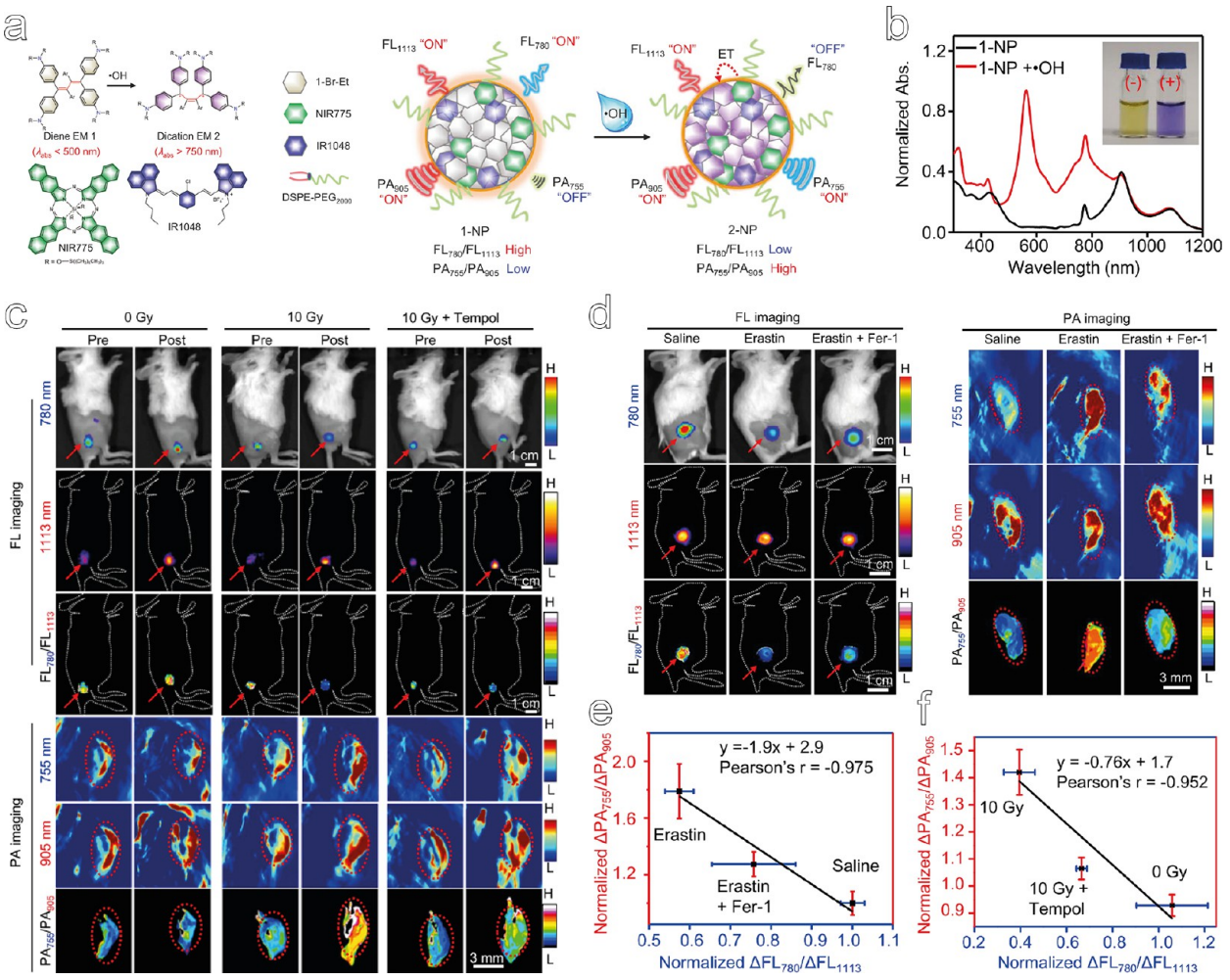

Figure 7. (a) Schematic illustration of the probe constituents and the mechanism of ratiometric visualization. (b) Normalized absorbance spectra of the probe, before and after incubation with •OH at room temperature. Inset: color change of the probe solution from yellow to blue-violet upon the addition of the analyte. (c) Fluorescence ($F^{ex:740}_{em:780}$ and $F^{ex:808}_{em:1113}$), photoacoustic (PA_{755} and PA_{905}), and their corresponding ratiometric images of 4T1 tumor-bearing mice. (d) Fluorescence, photoacoustic, and their corresponding ratiometric images of the mice treated with saline, erastin (ferroptosis inducer), and erastin plus ferrostatin-1 (ferroptosis inhibitor). Red arrows and dashed circles in frames (c) and (d) indicate the tumor site. The correlation between the ratiometric fluorescence and photoacoustic imaging in the mice undergoing (e) ferroptosis and (f) X-ray RT. Adapted with permission under a Creative Commons CC BY License from ref. 136. Copyright 2021 Springer Nature.

authors showed that the predicted NO level upon drug administration was in great consistency with the results obtained by measuring the expression level of M1-phenotype macrophage markers such as CD86, CD80, and iNOS, providing a reliable inspector for monitoring macrophage-mediated cancer treatment.[120] Moreover, by selecting other stimuli-responsive acceptors which ensured high spectral overlap with the afterglow substrate, they proved that the concept can be further extended to other important biotargets such as pH and $ONOO^-$, providing universal ARET-based RNPs.[120] It seems that in contrast to most of the afterglow agents whose structural inertness and the lack of sufficient active site limit their capability to incorporate responsive molecules, employing ARET strategy might offer extra available sites on the acceptor to be exploited for conjugating different molecules.

In contrast to their advantages, the contribution of self-illuminating techniques in *in vivo* RNPs seems to be limited, which might be due to the intrinsic challenges of such modalities. For instance, the signal outputs of bioluminescence depend on the redox reactions mediated by luciferase enzymes whose stability can be affected by environmental parameters as well as the availability of their short wavelength emissive substrates, which might also suffer from poor stability and cell compatibility.[128] While the issues might not pose major problems for qualitative imaging, they can prevent the corresponding probes from taking part in quantitatively measuring analytes, especially for *in vivo* deep-tissue imaging. However, the rapidly evolving fields of protein engineering and synthetic chemistry have led to the introduction of more stable enzymes and substrates with a longer wavelength emitting capability,[129,130] which might feed into further contribution of excitation-free techniques in ratiometric detection technology.

2.3. Dual-Modality RNPs. Dual-modality probes in which the ratiometric characteristics are merely afforded by one of the modes have been developed over the recent decade. For instance, the MMP-2 activatable sensor for fluorescence and photoacoustic imaging was developed by our group.[1] To construct the probe, Cy5.5 dye was attached to its quencher (QSY21) *via* MMP-2 labile peptide (Figure 5). Consequently,

https://doi.org/10.1021/acsnano.3c01641
ACS Nano XXXX, XXX, XXX−XXX

the presence of the enzyme could gradually revive the fluorescence mode of the dye, while the PA_{730} signal of the structure remained unchanged. On the other hand, the cleavage disrupted the quenching role of the quencher, leading to an increase in the fluorescence emission of Cy5.5, which in turn enhanced the tendency of the dye to radiatively dissipate energy rather than producing heat. As a consequence, the PA_{680} of the platform decreased. The alterations afforded PA-based *in vivo* quantification of MMP-2 expression in mice bearing 4T1 tumors such that PA_{680}/PA_{730} signal increased 1.5 times within 90 min, while the fluorescence mode merely served as an auxiliary technique for confirming certain properties of the prepared probe (*e.g.*, the capability of MMP-2 expressing cells to cleave the peptide).

Recently, dual-modality ratiometric probes have been successfully developed in order to concurrently take advantage of the prominent characteristics of each of the modalities and provide multiscale data at several spatial and temporal scales.[95,131−133] For example, through finely designing a core−satellite nanosystem, an activatable photoacoustic and surface-enhanced Raman spectroscopy (SERS) dual-ratiometric probe for *in vivo* detecting the hydrogen peroxide (H_2O_2) level was constructed (Figure 6). The structure incorporated a 2-naphthalenethiol (NAT) Raman marker in its core whose SERS intensity ($I_{1418\ cm^{-1}}$) was protected from environmental-induced alterations by employing successive protective layers. From inside to outside, the layers included a nanogapped Au shell, horseradish peroxidase (HRP)- and ABTS-doped mesoporous silica shell as well as Au nanoparticles grafted with 4-mercaptobenzonitrile (MBN), and 4-mercaptobenzoboric acid (MPA) molecules. The formation of numerous electromagnetic hot spots in the nanogapped Au shell and the plasmonic coupling between the outermost Au nanoparticles gave rise to an intensified $I_{2228\ cm^{-1}}$ SERS intensity as well as a strong NIR-II optical absorbance profile, providing PA_{1250} signal. Nevertheless, not only did the presence of H_2O_2 induce a reduction in $I_{2228\ cm^{-1}}$ by detaching the outermost Au nanoparticles through converting boronic ester linkages to phenols, but also triggered an HRP-mediated catalytic reaction to oxidize ABTS and produce a strong NIR-I absorber product, leading to the emergence of PA_{750}. The alterations along with the stable PA_{1250} and $I_{1418\ cm^{-1}}$ signal intensities afforded dual-ratiometric PA/SERS characteristics for real-time quantitative detection of H_2O_2 in mice suffering from peritonitis and bacteria-induced acute inflammatory skin diseases. Moreover, besides its favorable *in vivo* performance, the core−satellite nanoprobe also exhibited great potential for *in situ* diagnosing knee osteoarthritis, characterized by the elevated level of H_2O_2, in rabbits. During ∼30 min of the measurement, the $I_{2228\ cm^{-1}}/I_{1418\ cm^{-1}}$ and PA_{750}/PA_{1250} signals reached to 0.5 and 3.4 times of their initial values, respectively.[131]

X-ray radiotherapy (RT) is being clinically utilized to destroy tumor cells by inflicting direct DNA damage as well as indirect damages induced by the radiolysis of water molecules and production of the highly reactive •OH species.[134] On the other hand, the ferroptosis therapeutic method for triggering regulated cell death in cancer cells takes advantage of the iron-dependent lipid peroxidation reaction in which the free radicals such as •OH, H_2O_2, and O_2^- attack polyunsaturated fatty acids.[135] Thus, since the level of •OH in the tumor microenvironment of the patients treated by either RT or ferroptosis determines the efficacy of the treatment, developing noninvasive and real-time methods for screening the •OH level might provide physicians with a powerful tool to evaluate treatment response and necessity of further medical intervention. An electrochromic material (EM) structure (1-Br-Et) consisted of a butadiene scaffold with the capability of forming a dication EM structure (2-Br-Et) upon the reduction of its diene by •OH, was coencapsulated with two commercially available dyes, namely, NIR775 and IR1048, into DSPE-PEG-formed micellar nanoprobe (1-NP) (Figure 7). In addition, the probe achieved the ability of actively targeting folate receptors overexpressed on the surface of certain tumor cells by being further modified with folic acid on its surface (1-NP-FR). While the FL and PA signals attributed to IR1048 (*i.e.*, $F^{ex:808}_{em:1113}$ and PA_{905}) exhibited an "always on" characteristic during the process of •OH-induced oxidation, those of NIR755 (*i.e.*, $F^{ex:740}_{em:780}$ and PA_{755}) decreased and increased, respectively. This might be caused by transferring the energy from the dye to the newly formed 2-Br-Et in the micelle which had a good NIR-I absorptivity. Hence, the probe exhibited dual-ratiometric properties, in which the FL and PA modes could be independently employed to detect the level of •OH in LPS/PMA-stimulated RAW264.7 cells or tumor site of mice bearing 4T1 breast cancer during RT or erastin-induced ferroptosis. For instance, it was shown that compared to nonirradiated tumors, a 2.7-fold reduction in the $F^{ex:740}_{em:780}/F^{ex:808}_{em:1113}$ signal as well as a 1.4-fold enhancement in the PA_{755}/PA_{905} signal could be identified for tumor sites where received 10 Gy X-ray.[136]

Notably, great consistencies have been reported between the results derived under each mode of dual-modality RNPs, indicating that one specific modality can be employed to endorse the results of the others. Therefore, it might be assumed that such probes can make a more valuable contribution in realizing personalized therapy. Taking FL/PA dual-modality as an example, the mutual endorsement of the results might provide the physicians with reasonable assurance when it comes to compromise between the sensitivity of the detection and the penetration depth. Particularly, in case that the site needed to be screened is located in the ranges that cannot be visualized by NIR-II FL imaging, the physician might order the provider company to exclude the FL agent from the formulation, not to impose unnecessary expenses on the patient.

3. MINIMIZING FALSIFIED SIGNALS GENERATED BY RNPS

As mentioned earlier, the complexities of biological microenvironments might complicate the accurate *in situ* quantification of a specific analyte within a living system. For instance, various known or unknown processes might get involved in the progression of the diseases which can dynamically change the concentration of the analyte of interest. In addition, the biological environments might offer substances (*e.g.*, proteins, lipids, biomolecules) which can interfere with the detecting mechanism of the designed probes. This might happen through the capability of the interfering substances to compete with the analyte of interest for the recognition sites of the probes or *via* altering the physiochemical characteristics of the nanosystems. Regardless of the origin of such interferences and complications, the results obtained from the measurement might contain falsified information. In this section, the recent innovative approaches to maximize the accuracy of data obtained from the biological environment is reviewed. It is worth noting that although a few of the RNPs introduced in

https://doi.org/10.1021/acsnano.3c01641
ACS Nano XXXX, XXX, XXX−XXX

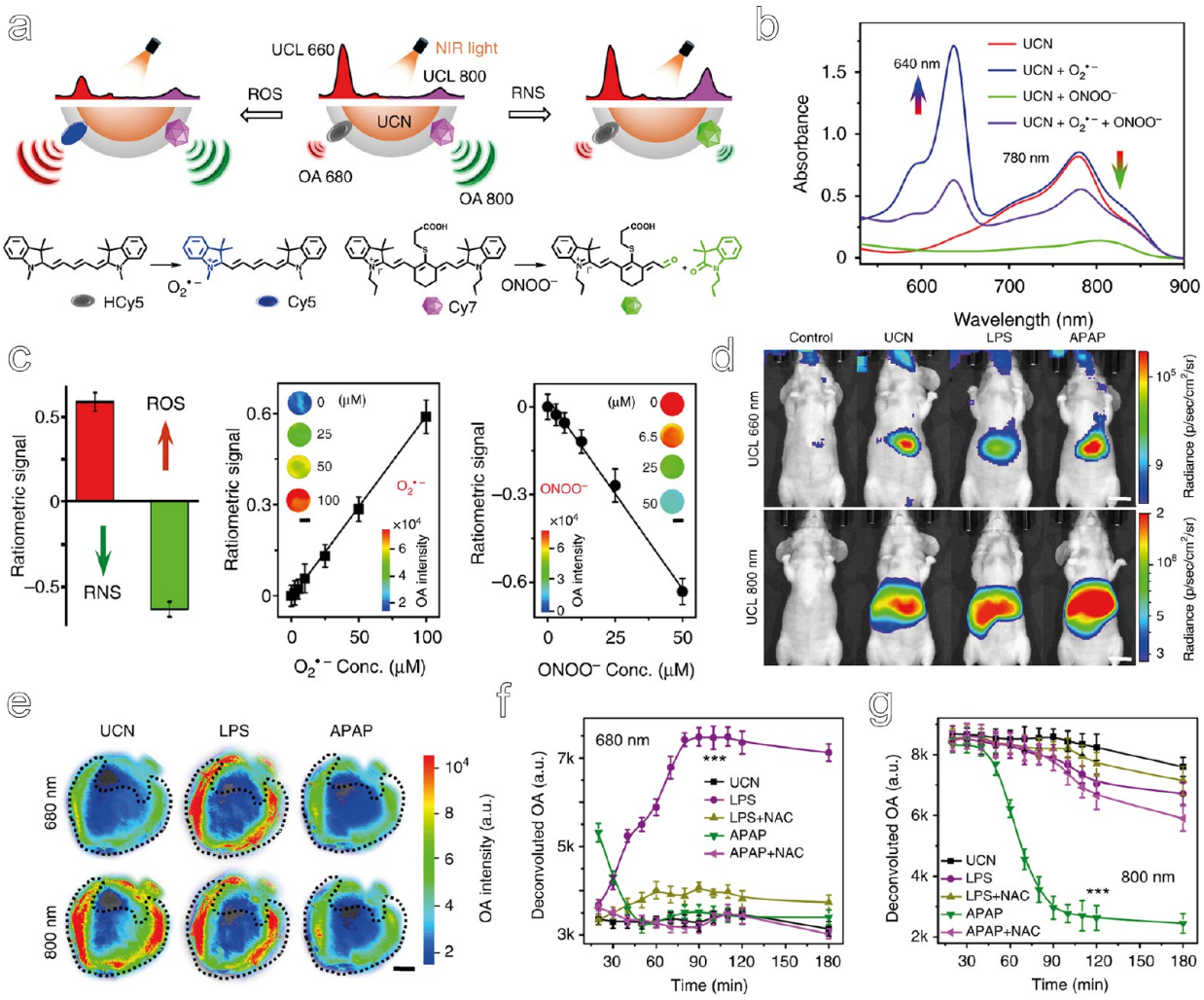

Figure 8. (a) Schematic illustration of probe design and the mechanism of ratiometric ROS and/or RNS detection. (b) Absorbance spectra of the probe upon being treated with ROS and/or RNS. (c) Deconvoluted ratiometric optoacoustic (OA) signals in the absence (OA_0) or presence (OA_1) of ROS and RNS (left). Ratiometric analyses performed by employing the $\Delta OA_{680} + \Delta OA_{800}/\Delta OA_{800}$ formula. Ratiometric signal variation in response to the addition of ROS (middle) and RNS (right) at different concentrations. (d) Variation of $F^{ex:980}_{em:660}$ and $F^{ex:980}_{em:800}$ signals upon treating the models with saline (control), UCNs, LPS, and APAP for 90 min. (e) ΔOA_{680} and ΔOA_{800} in the region of interest within liver tissue, following *in vivo* treatment of the model with UCN, LPS, and APAP for 90 min. Temporal variation of deconvoluted OA signals in the 680 nm (f) and 800 nm (g) channels, for hepatic inflammation models treated with UCNs, LPS, APAP and their corresponding metabolite scavengers. Scale bars in frame (d) and (e) represent 1 cm and 5 mm, respectively. Adapted with permission under a Creative Commons CC BY License from ref. 139. Copyright 2019 Springer Nature.

this section might possess some features that enable them to be categorized under certain above-mentioned subsections as well, the themes of their corresponding studies suggest a higher degree of overlap with the concept of the current section.

3.1. Dual-Responsive RNPs. Thus far, the activatable ratiometric probes that also have the capability of targeting the tissues of interest through active targeting have been shown to be promising for minimizing the false positive or negative signals. On the other hand, the tumor-specific biomarkers are multifaceted and might be interconnected with each other. It has been proven that the abnormalities of the tumor might have a synergic effect when they coexist, which leads to more severe effects if they happened individually. Therefore, developing dual-target triggered RNPs might shed more light on the correlations between these hallmarks in the microenvironment of chronic diseases in order to gain more information about their progression and come up with better solutions to efficiently treat them.[7,137−139]

Taking advantage of the dual-channel emitting capability of Ln-doped upconversion nanocrystals (UCNs), a platform for concurrently screening the level of superoxide anion ($O_2^{\bullet-}$), $ONOO^-$, and their interrelation was developed by our group.[139] To this end, the ROS-sensitive HCy5 and RNS-responsive Cy7 fluorophores whose absorption profiles overlap with $F^{ex:980}_{em:660}$ and $F^{ex:980}_{em:800}$ of UCNs, respectively, were anchored to the surface of the nanoparticle (Figure 8). Upon NIR laser excitation and the presence of the species, the manner with which the energy transferred from the excited UCNs to the fluorophores gave rise to distinctive alterations in their PA signals, endowing the platform with disparate ratiometric characteristics for each of the analytes. Utilizing the probe, we could simultaneously and orthogonally quantify the oxidative and nitrosative stresses triggered by endogenous redox agents, with outstanding spatiotemporal resolution in living mice.

Ratiometric MRI contrast agents have been developed by exploiting the degradability of magnetic metal oxide nanoma-

https://doi.org/10.1021/acsnano.3c01641
ACS Nano XXXX, XXX, XXX−XXX

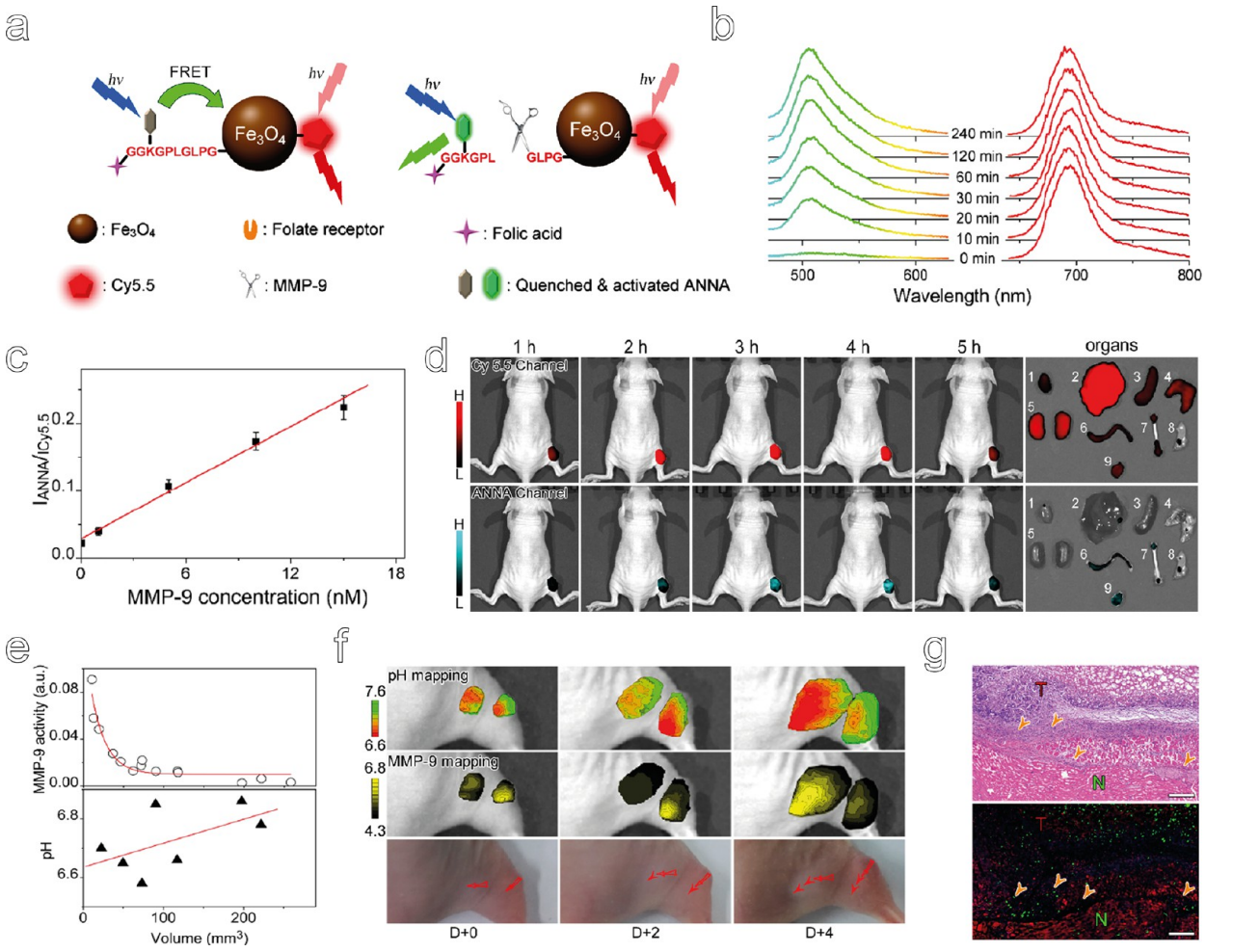

Figure 9. (a) Schematic illustration of probe constituents and the mechanism of MMP-9 detection. (b) Variation of fluorescence intensity for $F^{ex:455}_{em:510}$ and $F^{ex:650}_{em:700}$ signals upon incubating the probe with MMP-9 for different time intervals. (c) Ratiometric ($F^{ex:455}_{em:510}/F^{ex:650}_{em:700}$) fluorescence intensities of the probe as a function of MMP-9 concentrations. (d) Temporal fluorescence intensity arising from the tumor site, in the Cy5.5 and ANNA channels. The right panel represents the fluorescence signals arising from major organs collected from the sacrificed animals, in the corresponding channels (1−9: heart, liver, spleen, lung, kidney, intestine, bone, muscle, and tumor). (e) Quantified expression level of the enzyme (upper panel) and acidity (lower panel) within the tumor microenvironment, obtained by employing multimodality imaging and ANNA emission, respectively. (f) Quantified pH and enzyme mapping within the tumor site and the growth direction of the tumor, during 4 days. (g) Upper panel: H&E staining for a tissue slice. Lower panel: merged immunofluorescence staining of two adjacent slides stained for E-cadherin expression (red) and MMP-9 expression (green), respectively. The arrows indicate the boundaries between the tumor and healthy tissues where the enzyme is highly expressed. The scale bar represents 200 μm. Adapted with permission from ref. 7. Copyright 2018 American Chemical Society.

terials (MMONPs) into free metal ions and water molecules, under conditions characterized by low pH and high H_2O_2 concentration. Although MMONPs are known as negative contrast agents for T_2-weighted MRI, the release of metal ions would not only simultaneously lead to a decrease in T_2 and an increase in T_1 signals,[140] but also can mimic Fenton reaction and trigger a chemodynamic effect by inducing intracellular oxidative stress.[141] Thus, cobalt oxide (Co_3O_4) nanoprisms possessing photothermal characteristics were loaded with doxorubicin (DOX) to prepare a platform for ratiometric monitoring of H_2O_2 and pH level as well as exerting concurrent photothermal, chemodynamic, and chemotherapeutic effects. The probe could successfully visualize the level of analytes in human colorectal carcinoma-bearing mice and induce tumor ablation.[142]

Since the state of spatiotemporal heterogeneity in the properties of a tumor can affect the therapeutic administration, noninvasively quantifying the feature is highly valuable. Through an antibody-conjugated MMP-9 cleavable peptide, Fe_3O_4 nanoparticles were covalently attached to molecules of a fluorescent dye, namely, 3-amino-1,2,4triazole-fused 1,8-naphthalimide (ANNA). Due to the broad absorption profile of Fe_3O_4 covering the emission of the dye, the fluorescence of ANNA in the absence of MMP-9 was expected to be in "off" state, regardless of the pH value. In the presence of the enzyme and upon the cleavage of the linking peptide, the fluorescence got revived and exhibited an increasing trend in its $F^{ex:455}_{em:480}$ signal and a stable $F^{ex:455}_{em:510}$ signal, in response to the reduction in pH value from 7.1 to 5.7. By taking the interaction of light with tumorous and its surrounding healthy tissues into consideration, the authors could semiquantitatively correlate the 2D fluorescence imaging results with the 3D heterogeneous structures of tumor in order to endow the probe with pH mapping capability.[143] However, although the accurate *in vivo* binding kinetics of antibody−antigen is not well-understood, it is presumable that some of the dye−antibody conjugates tend

https://doi.org/10.1021/acsnano.3c01641
ACS Nano XXXX, XXX, XXX−XXX

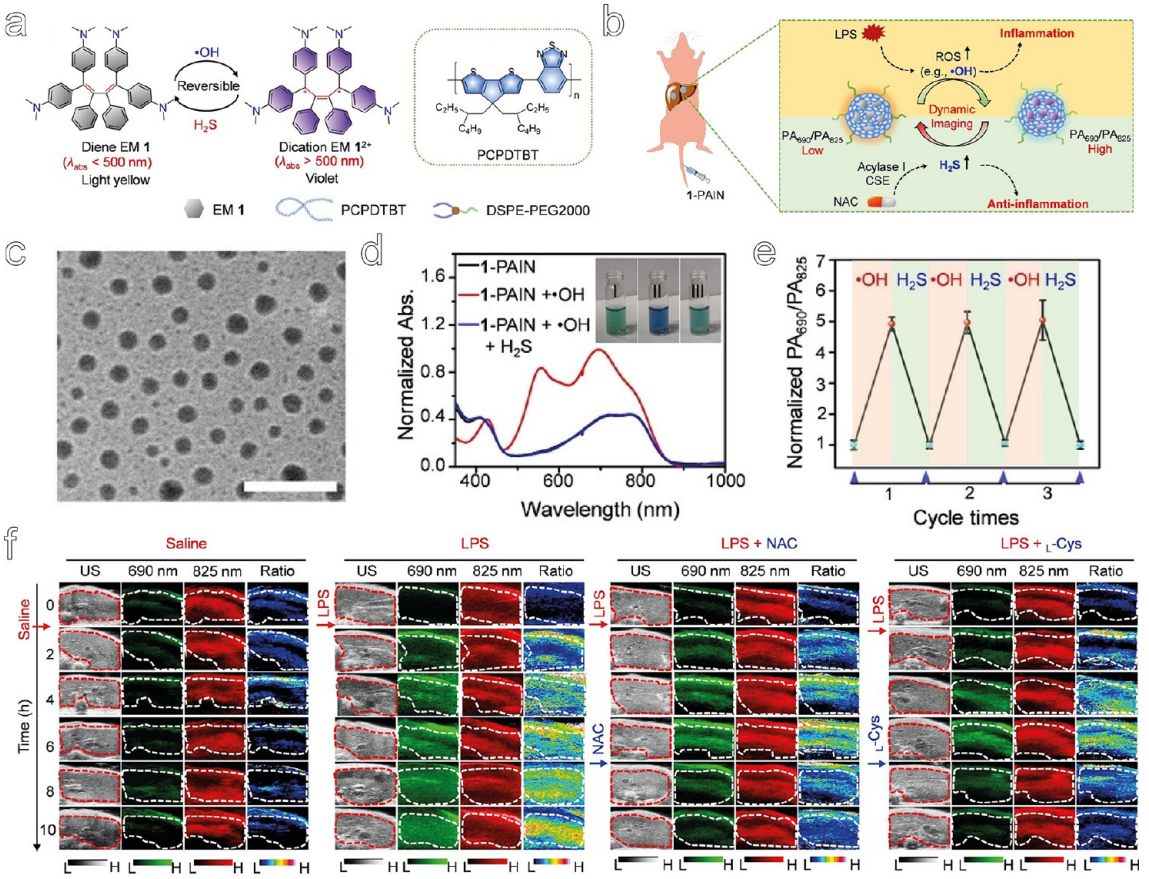

Figure 10. (a) Schematic of the chemical structures of EM 1, EM 1^{2+}, PCPDTBT, and the mechanism of reversible detection of •OH and H_2S. (b) Mechanism of ratiometric photoacoustic imaging during LPS-induced inflammation and NAC-triggered anti-inflammatory responses in liver upon intravenous injection of the probe. (c) TEM image of the probe. Scale bar represents 200 nm. (d) Normalized absorbance intensities of the probe in response to the analytes. (e) Normalized ratio of the photoacoustic signals upon exposure to three cycles of successive •OH and H_2S addition. (f) PA_{690} (green), PA_{825} (red), and their ratio (PA_{690}/PA_{825}) collected from liver of mice following treatments with saline, LPS, LPS+NAC, and LPS+L-Cys. The liver borders and the regions of interest for analyzing the signals have been indicated by red and white dashes, respectively. Adapted with permission from ref. 151. Copyright 2022 John Wiley and Sons.

to detach from the surface antigen after some time of residence, diffusing toward the surface of the tumor and its surrounding healthy tissues with a diffusion coefficient which is difficult to be obtained. The challenges impair the pH imaging contrast for prolonged monitoring and makes the correlation between pH imaging and the heterogeneity of the tumor difficult. By introducing pH- and MMP-9-insensitive Cy5.5 dye ($F^{ex:650}_{em:700}$) to the ANNA-Fe_3O_4 probe, our group employed a similar strategy to gain a better understanding of the *in vivo* correlation between pH and MMP-9 (Figure 9). The design allowed obtaining an on/off ratio of 17 within 4 h for the fluorescence intensity attributed to ANNA, while the intensity of $F^{ex:650}_{em:700}$ did not encounter any noticeable variation. The obtained results from the prepared RNP as well as those of histopathological and immunohistochemical analyses confirmed that although the probe homogeneously distributed within the tumor, the expression of MMP-9 and also the lowered value of pH were consistently heterogeneous. Moreover, not only were the levels of two abnormalities strongly correlated, but also they had a synergic effect on the metastatic nature of the tumor and could drop a hint about the direction of tumor motility in a spatiotemporal manner.[7]

Differentiating $ONOO^-$ from the hypochlorite ion (ClO^-) and also inspecting the correlation between abnormal levels of the two species are of great physiological and pathophysiological importance.[144] Employing an alkyl chain linker, a ClO^- responsive precursor (phenothiazine-based coumarin) whose sulfur atom was prone to be rapidly oxidized by ClO^- was fused with an $ONOO^-$ sensitive carrying structure (2(benzo-[d]thiazol-2-yl)aniline) in which the benzyl boronic ester unit underwent a cleavage reaction in the presence of peroxynitrite. The variations in intramolecular charge transfer associated with the separate or concurrent existence of the analytes in the environment-induced spectral shift(s) in the fluorescence profile of the probe. The luminophore precursors were selected as such to provide minimum spectral crosstalk, endowing the probe with the capability of ratiometrically detecting the solely- or coexistence (regardless of the order of introduction in the environment) of ClO^- and $ONOO^-$ in LPS/PMA-induced inflammatory RAW 264.7 cells and zebrafishes.[145]

Being the main components of proteins makes L-amino acids inseparable elements for certain physiological activities in biological systems. For instance, L-lysine (L-Lys) is one of the essential amino acids that is not synthesized by the human body and has to be supplied by one's diet. On the other hand, both the excess and shortage of the amino acid might be a signature or the cause of some medical complications, such as anemia, hair loss, hyperlysinemia, cystinuria, Alzheimer's, *etc.*, highlighting the importance of developing methods for

https://doi.org/10.1021/acsnano.3c01641
ACS Nano XXXX, XXX, XXX−XXX

accurate and rapid detection of L-Lys.[146] It is important to note that the detection techniques should afford enantioselective identification in order to differentiate the analyte from its enantiomer which might have inconsistent or even opposite physiological functions.[147] In an attempt to develop such probes, Chang et al. adopted a hydrothermal method to synthesize dual-emission carbon dots (CDs) out of urea and a phenazine dye (neutral red) as precursors, providing a structure with a fluorescence quantum yield (QY) of 32% and the capability of concurrent detection of pH and L-Lys. The free amino group of L-Lys is located relatively far from its zwitterionic center, facilitating the hydrogen bond formation between NH_3^+ of the amino acid and oxygen-containing groups (−COOH and −OH) which are usually abundant on the surface of measuring probes.[148] Following the hydrogen bond formation and as a consequence of an enhancement in the π-conjugation as well as a restriction in vibrations of CDs' functional groups, the intensity of $F_{em:440}^{ex:380}$ signal increased while that of $F_{em:542}^{ex:380}$ remained invariable. However, the exact opposite trends in fluorescence intensities were observed in response to increasing pH from 2 to 8, providing the possibility of concurrent monitoring of pH and L-Lys level in HeLa cells and also living zebrafishes.[149]

3.2. RNPs with Dynamic Response. Living organisms are characterized by the existence of numerous biological entities and the occurrence of a great deal of biological events that might dynamically interact with one another under different environmental parameters either to perform specific functions or as a response to external stimuli. The subtle interplay of the entities, regardless of being advertent or fortuitous, introduces enormous complexity to biological systems, complicating the close *in situ* inspection of a specific biological event of interest. For example, upon the occurrence of oxidative stress and as a result of the vital and dynamic processes in order to restore the disturbed balance between cellular oxidant and reductant couples, the concentration of these couples might change spatiotemporally within living organisms.[150] This fact highlights the importance of endowing RNPs with the capability of detecting analyte concentration in a reversible manner, which has been accomplished by some researchers.[151−157] In contrast to those RNPs whose analyte-sensitive moieties undergo irreversible cleavage during the recognition process, the RNPs with dynamic response might make a more significant contribution to long-term *in vivo* inspection of tissues of interest.

As one of the most reactive species, •OH is known as highly toxic with the capability of triggering oxidative stress following the reaction with a variety of endogenous biomolecules. On the other hand, together with NO and carbon monoxide (CO), H_2S is recognized as an important endogenous gas neurotransmitter (gasotransmitter) and a potent reducer that plays a vital role in many physiological and cytoprotective functions.[158,159] In contrast to a healthy liver, the ROS level gets elevated in hepatitis during the inflammatory progression.[160] Following the administration of N-acetyl cysteine (NAC) as an anti-inflammation drug, acylase I metabolizes the drug into L-cysteine, which in turn can be converted into H_2S by cystathionine-γ-lyase (CSE).[161] Thus, the real-time inspection of the fluctuation in the concentration of •OH/H_2S redox couple is of great importance to reflect the degree of liver inflammation as well as evaluate the potency of the administered anti-inflammation drugs in individual cases. The NIR absorption profiles of the EMs composed of organic π-electron structures are subjected to reversible alteration in response to fluctuation in the level of •OH and H_2S, making the materials great candidates for photoacoustic imaging of the redox couple. The structure of EMs was designed such that the rapid and selective oxidization by •OH rendered the diene structure (EM 1) into dication form (EM 1^{2+}) while H_2S-induced reduction could rapidly switch the structure back to EM 1 (Figure 10). Following the reversible structural transformation, the initially weak PA_{690} signal encountered a successive increase and decrease with regards to sequential •OH oxidization and H_2S reduction, respectively, in an "off−on−off" manner for PA_{690} signal. On the other hand, incorporating a semiconducting polymer (PCPDTBT) together with the EM 1 structure into a DSPE-PEG micellar system provided the "always on" reference PA_{825} signal due to the insensitivity of the polymer to most of the biological and physiological hallmarks.[162] Thus, upon •OH-induced oxidation of the structure, the value of PA_{690}/PA_{825} reached 5 times its initial level, and then switched back to the initial value following the H_2S-induced reduction. It was shown that the prepared reversible ratiometric imaging agent could successfully realize the real-time diagnosis of LPS-induced liver inflammatory process and the successive drug-induced anti-inflammation hepatic response through the noninvasively monitoring of •OH/H_2S fluctuation.[151]

Boron dipyrromethene (BODIPY) dye was employed as a chemical skeleton and formed a micellar structure by using DSPE-PEG, in order to dynamically monitor the interaction between superoxide $O_2^{\bullet-}$ and glutathione (GSH) as a natural redox couple within our bodies. The ortho-phenolic hydroxyl group on the skeleton underwent an oxidation reaction with $O_2^{\bullet-}$, inducing antagonistic trends in the photoacoustic signals of the dye (*i.e.*, PA_{680} and PA_{750}). On the other hand, the oxidized form of the probe could be readily reduced by GSH, reversing the $O_2^{\bullet-}$-associated alterations made in the photoacoustic signals.[163] The nanomicelle was successfully employed to visualize the localized redox homeostasis between the species in EMT6 tumor-bearing mice following the successive treatment of the animals with phorbol myristate acetate (PMA) and α-lipoic acid (LPA) as the inducers of $O_2^{\bullet-}$ and GSH species. Particularly, it was shown that PA_{750}/PA_{680} signal for mice treated with PMA underwent a 6.3-fold enhancement, then encountered a reduction following the treatment of the animals with LPA, confirming the capability of the probe in visualizing the dynamic interaction of the analytes.[153]

Spiro rings that can be reversibly opened and closed in response to the acidity of microenvironments have been exploited to design pH-activated RNPs.[164−168] For example, a structure consisting of a tetrastyrene unit and rhodamine was constructed in which the spirolactam ring of the latter got open in media with lowered pH values (from 8 to 2). Consequently, the FRET mechanism was triggered between the constituents and led to a reduction in the intensity of the initial $F_{em:455}^{ex:380}$ signal and emergence of the $F_{em:593}^{ex:380}$ signal. It was shown that the probe could ratiometrically and dynamically determine the pH level in zebrafish.[167] In addition, quinoline units might also be able to serve as proton recognition sites in a dynamic manner. For instance, following the protonation of quinoline moiety incorporated in a chemical conjugation consisting of methyl carbitol-substituted carbazole, the electron-withdrawing ability of the moiety was intensified and resulted in an enhancement in ICT mechanism. Thus, a red shift in the fluorescence profile was achieved (*i.e.*, from $F_{em:530}^{ex:415}$ to $F_{em:637}^{ex:415}$),

https://doi.org/10.1021/acsnano.3c01641
ACS Nano XXXX, XXX, XXX−XXX

and the signals were employed for *in vivo* observation of pH alteration in LPS-induced inflammation in mice models. However, the process could be reversed in response to the deprotonation of the moiety, affording a dynamic response.[169] Deprotonation of hydroxyl groups in the presence of OH^- is another method with which ratiometric pH sensors for *in vivo* applications have been designed.[170,171] To take advantage of this property, a probe based on rhodamine derivative containing an electron donor (phenolic hydroxyl) and a positron acceptor (nitrogen) was designed. It was demonstrated that the deprotonation of the hydroxyl would lead to an enhancement in the ICT process between the donor and the acceptor as well as a reduction in the energy level gap between HOMO and LUMO. The consequent redshift from $F^{ex:530}_{em:586}$ to $F^{ex:530}_{em:628}$ induced by elevating the pH value from 5.8 to 10.0 led to a 20-times enhancement in the $F^{ex:530}_{em:628}/F^{ex:530}_{em:586}$ signal. The strategy was shown to be effective in ratiometrically observing pH levels in living cells and zebrafishes as well as during autophagy in mitochondria.[170]

3.3. RNPs for Neutralizing Microenvironmental-Induced Interferences. The susceptibility of certain analytes of interest to be scavenged by specific *in situ* compounds or the dependency of their activities on environmental parameters, such as pH, might result in falsified sensor response and misleading output. For instance, the *in situ* catalytic activity of the majority of peroxidase mimetics can be suppressed due to the discrepancy between the intracellular pH and the favorable pH for the occurrence of the catalytic reaction.[172,173] In addition, the intermediates or the final products of the catalytic reaction are prone to be reduced by GSH, prior to being identified by the sensor.[174,175] To address the challenges, developing advanced strategies for alleviating the effect of unwanted reactions by providing a favorable microenvironment for optimal functioning of RNPs as well as protecting the reaction products from being altered before the completion of the transduction process might be helpful to neutralize the microenvironment-disruptive interferences.

Inflammation can be attributed to the deviation of the ROS level from their physiological concentrations in a specific part of our bodies.[176] Real-time and quantitative visualization of the inflammatory response during the process of treatment is considered an effective method for early prediction of the treatment efficiency. However, the persistent incidences of inflammation in the neighboring areas around the location of interest inevitably impose signal disruption and falsified output. For example, bone repair consists of several stages among which inflammation, angiogenesis and bone remodeling can be mentioned. Disturbance in either of the stages can lead to abnormalities such as the dissolution of bone minerals and degradation of organic bone matrix in response to inflammation dysregulation, skeletal diseases caused by the lack of sufficient newly formed vasculature as well as implant degradation in the remodeling stage.[177] The swelling of tissues surrounding the bone hinders the accurate inspection of inflammatory response during the bone repair process. To address the issue, bioactive glass (BG) scaffolds containing hexagonal-phase $NaErF_4@NaYF_4$ (ErNPs) were prepared whose surfaces were further engineered with a hypochlorous acid (HClO)-bleachable IR808 dye. Although the intensity of $F^{ex:808}_{em:1525}$ arising from ErNPs was suppressed due to the IF effect exerted by the presence of IR808, the bleaching of the dye by HClO could limit the competition in favor of ErNPs and revive the intensity. Meanwhile, the $F^{ex:980}_{em:1525}$ signal of ErNPs did not show any sensitivity toward the analyte, serving as the reference signal. Following the *in situ* implantation of the scaffold in mice with bone defects, the ratiometric feature of the platform could successfully assist in sensitive mapping of inflammation by detecting the HClO concentration in the tissue microenvironment. Moreover, long-term angiogenesis and bone remodeling stages could also be visualized through the absolute intensity-dependent signal readout of the platform. The authors also reported that not only the host matrix of the scaffold showed excellent osteogenic performances, but also it protected the emission of ErNPs from the water quenching effect as well as reduced the interference of tissue swelling-induced signal fluctuation. It indicated that a lower power density of laser could be adjusted, which in turn led to the lower IR808 photobleaching as well as a reduction in thermal damage to healthy tissues by a laser-induced overheating effect.[94]

As another attempt to minimize the interference of the tissue swelling-induced signal in the process of quantification of ROS-induced inflammation, Li *et al.* developed MRI-based RNPs for predicting the therapeutic efficiency of inflammatory therapy in early stages. Hollow mesoporous silica nanoparticles (MSN) doped with manganese were grafted by tempol as ROS scavengers and coated with a porous, ROS-permeable platelet membrane as the active targeting agent for inflammation regions based on its high affinity toward the von Willebrand factor. Following the degradation of the structure triggered by the elevated acidity and ROS level, the covalent bond between the silica framework and manganese dissociated to release Mn^{2+} ions, turning the T_1-weighted MRI signal "on" in such a way that the signal intensity positively correlated with the degree of abnormalities in pH and ROS levels. More specifically, the probe could quantitatively assess the state of inflammation in acute liver failure (ALF) and acute pancreatitis (AP) animal models by taking advantage of the linear relationship between the variation in longitudinal relaxivity (ΔR_1) and the concentration of H_2O_2, a well-known hallmark of the ALF and AP.[178] Since the decrease in the concentration of transaminases in blood serum can be attributed to the recovery or exacerbating the hepatic and pancreatic failure, monitoring the biochemical indicators in blood samples might easily lead to subjective misinterpretation about the disease progression.[179] Therefore, Li *et al.* showed that compared to the conventional biochemical tests, analyzing inflammation-induced ROS provided a more accurate and reliable strategy to identify the progression stage of the disease, offering more appropriate and personalized treatment approaches.[180] Moreover, the capability of MSN to mimic a Fenton reaction in order to decompose H_2O_2 into oxygen and also the ability of tempol molecules to scavenge $O_2^{\bullet-}$ and •OH enabled the probe to exhibit radical-scavenging property and suppress the hypoxia-inducible factor (HIF-1α) in the inflammatory region, which in turn could alleviate oxidative stress and protect tissue against attributed damages.[180]

Apart from the variation of R_1 employed in the above-mentioned study, our group showed that the alteration in both the longitudinal and transversal relaxivities (ΔR_1 and ΔR_2, respectively) could be quantitatively attributed with GSH concentration.[181] To this end, ultrasmall Fe_3O_4 nanoparticles were first coated with maleimide groups. Subsequently, the resulting product was further conjugated to a ligand in which RGD and angiopep-2, as the targeting and BBB permeable peptides, respectively, were fused through a disulfide bond

https://doi.org/10.1021/acsnano.3c01641
ACS Nano XXXX, XXX, XXX−XXX

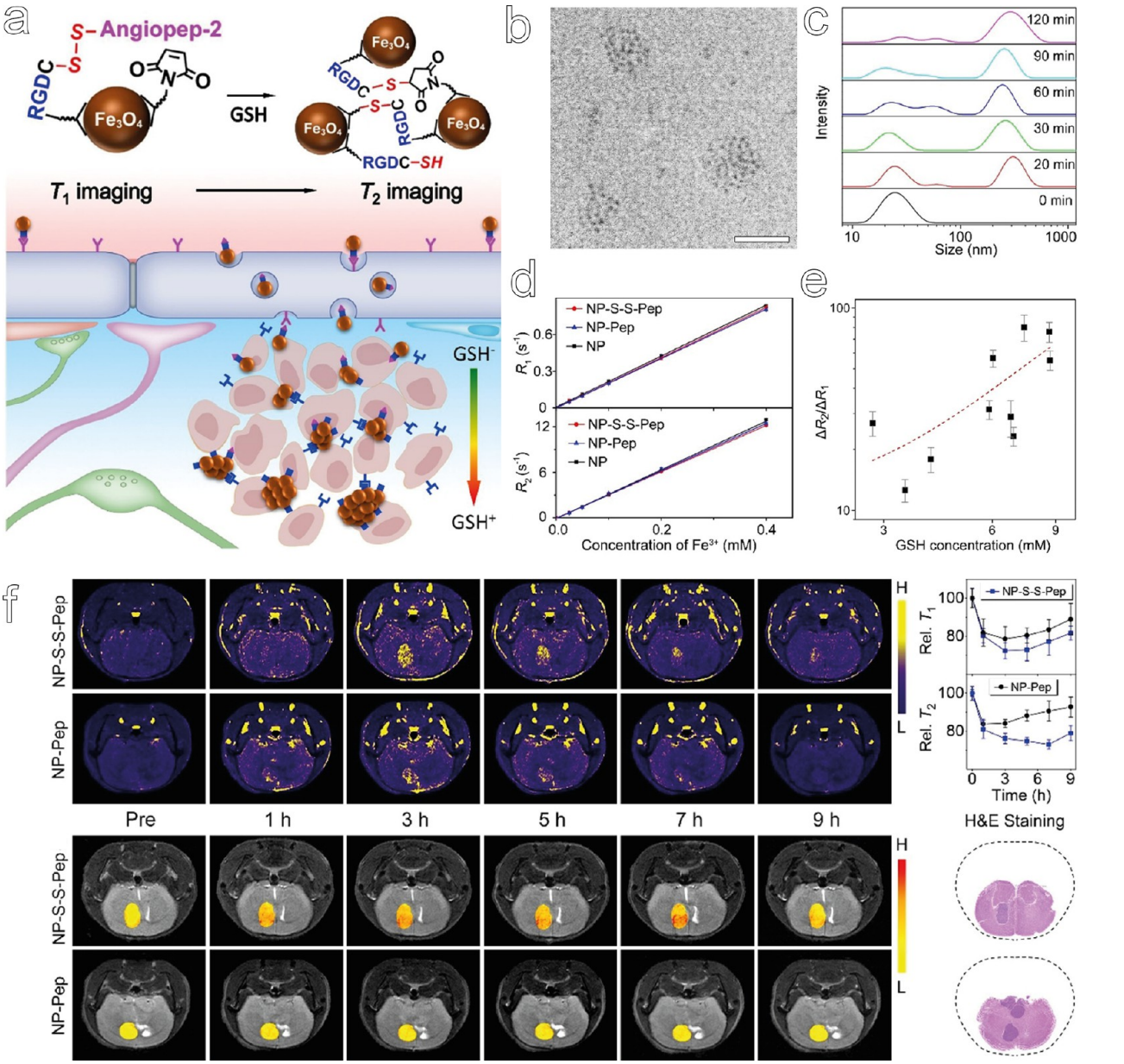

Figure 11. (a) Schematic illustration of probe design and the aggregation formation in the presence of GSH. (b) TEM image of the probe following GSH-induced agglomeration. Scale bar represents 30 nm. (c) Temporal variation in hydrodynamic size upon incubating the probe with GSH for different time intervals. (d) Variations and corresponding linear fittings for R_1 and R_2 values, as a function of iron concentration. (e) The experimental $\Delta R_2/\Delta R_1$ values for the tumor site of mice bearing subcutaneous xenografts, as a function of tumor GSH contents determined by ELISA. The dashed line represents the theoretical fitting obtained by the mathematical model. (f) *In vivo* MR imaging of intracranial tumors at different time points postinjection of probes. NP-S-S-Pep and NP-Pep indicate GSH-sensitive and GSH-insensitive probes, respectively. Upper and lower panels represent T_1- and T_2-weighted images of mice bearing orthotopic U87MG glioblastoma xenografts. Right-top represents relative T_1 and T_2 values recorded from the tumor site at the time points. Right-bottom represents H&E staining of brain slices. Adapted with permission from ref. 181. Copyright 2021 John Wiley and Sons.

(Figure 11). In the tumor microenvironment, a GSH-mediated redox reaction led to the cleavage of the bond between the peptides, preparing reactive thiol groups on the surface of the probe, initiating a particle aggregation through interparticle cross-linking of the thiol with maleimide groups on the adjacent particles.[182] This resulted in a reduction in surface area and total hydration number of the magnetic particles, leading to reversed variation tendencies in R_1 and R_2 values with respect to GSH concentration. Subsequently, a mathematical model was established to quantitively visualize the *in vivo* GSH heterogeneous distribution within brain gliomas tumor. It was shown that there was a great consistency between the results predicted by the model and those derived from immunohistochemistry analyses. Interestingly, we identified that the tumor regions with higher proliferation activity exhibited higher GSH concentration.[181]

The challenges such as low stability, relatively big size and high cost of the natural enzymes have spread the interest in developing and optimizing enzyme mimetic compounds in the past few decades. For instance, with the help of simulating natural peroxidase enzymes, nanosystems for catalyzing the oxidation of peroxidase substrates have emerged and exploited

https://doi.org/10.1021/acsnano.3c01641
ACS Nano XXXX, XXX, XXX−XXX

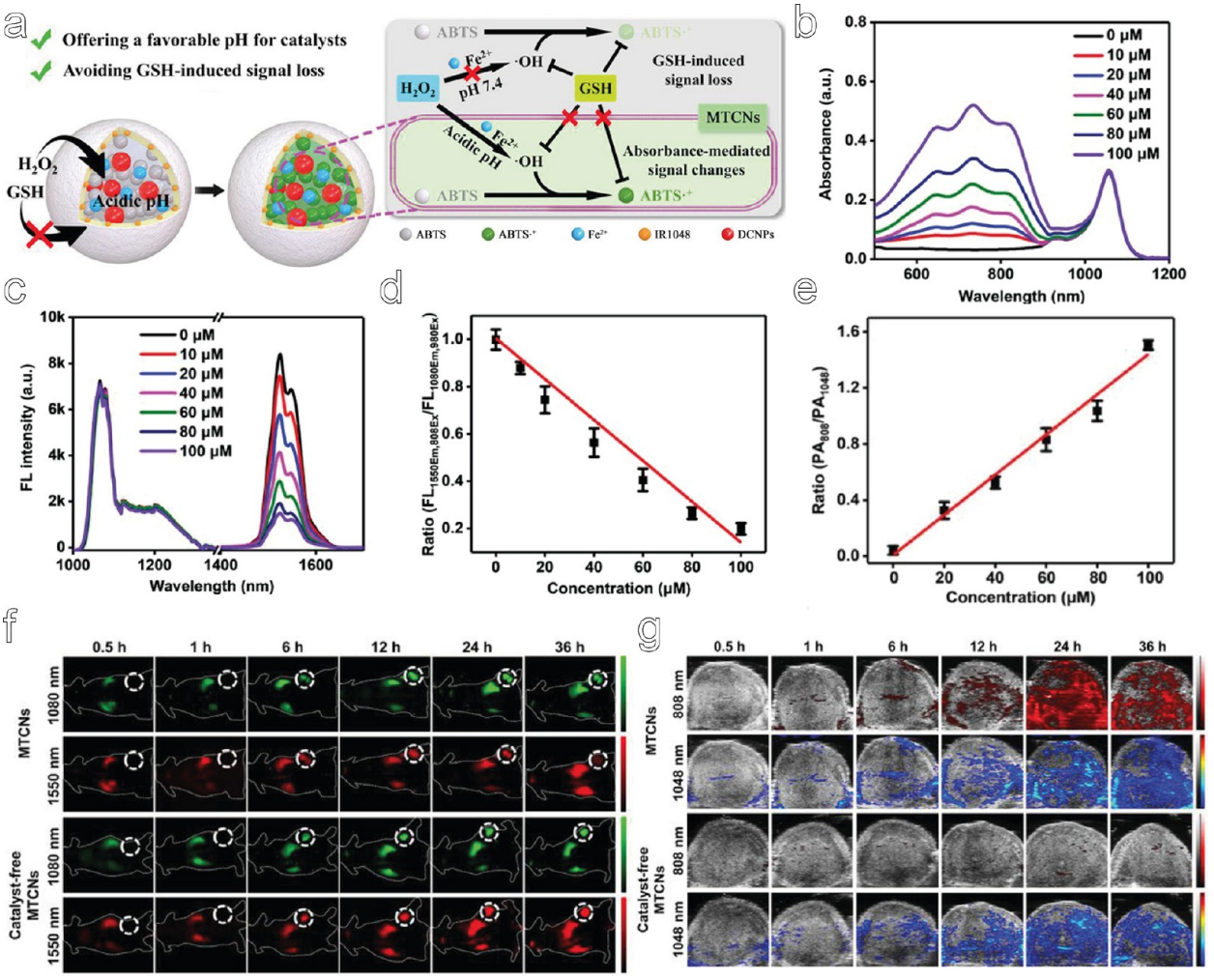

Figure 12. (a) Schematic of microenvironment tailored catalytic nanoprobes (MTCNs) for providing favorable pH and protecting the reaction intermediates from the microenvironmental interfering species. Variation of (b) absorbance and (c) fluorescence spectra in response to different concentrations of H_2O_2. Linear relationship between (d) $F^{ex:808}_{em:1550}/F^{ex:980}_{em:1080}$ and (e) PA_{808}/PA_{1048} versus different concentrations of H_2O_2. Quantification of the concentration of H_2O_2 in 4T1 tumor-bearing mice *via* ratiometric (f) NIR-II fluorescence imaging and (g) photoacoustic imaging upon intravenous injection of MTCNs and catalyst-free MTCNs as the control. Adapted with permission from ref. 95. Copyright 2022 John Wiley and Sons.

for the detection of H_2O_2 through converting it to other ROS and the subsequent transduction into a measurable signal.[183] Nevertheless, the optimal pH required for the efficient performance of the nanosystems might not always be provided by the complex intracellular microenvironment of the tissue. In addition, ROS generated in the catalytic reaction are susceptible to be scavenged by the cellular reductants such as GSH,[184] falsifying the signal output. In an attempt to address the issues, Chen *et al.* came up with the idea of microenvironment tailored catalytic nanoprobes. To this end, liposome-based nanoprobes were constructed such that its lipid membrane incorporated with NIR-II dye IR1048 and its hydrophilic cavity was loaded with ferrous ions (Fe^{2+}), citric acid (CA), 2,2′-azino-bis(3-ethylbenzothiazoline-6-sulfonic acid) diammonium salt (ABTS), and PEGylated DCNPs ($F^{ex:808}_{em:1550}$). While Fe^{2+} catalyzed the oxidation reaction between ABTS and H_2O_2 in the satisfactory acidic pH provided by CA inside the cavity, the liposomal lipid membrane protected the intermediate products (*i.e.*, •OH and ABTS•$^+$) from being reduced by GSH, providing a tailored microenvironment for H_2O_2 sensing in a wide range of pH values (Figure 12). This achieved by the permeability of the membrane to H_2O_2 and its impermeability toward hydrophilic ions and molecules. Although the intensity of the IR1048 fluorescence signal ($F^{ex:980}_{em:1080}$) and that of its photoacoustic signal (PA_{1048}) remained unchanged, the production of ABTS•$^+$, which showed a strong absorbance at 808 nm, fostered competition among the intermediate and DCNPs for the excitation light, resulting in a sharp reduction in the intensity of $F^{ex:808}_{em:1550}$ as well as a noticeable increase in the photoacoustic signal of the nanoprobe at 808 nm (PA_{808}). The reference and altered signals gave rise to a dual-ratiometric H_2O_2-responsive probe with the feasibility of inactively targeting the tumor site of mice bearing 4T1 breast cancer in order to precisely visualize the level of intratumoral H_2O_2. Moreover, contrary to the mice with healthy sentinel lymph nodes (SLNs), the injection of the probe to the mice suffering from metastatic SLNs led to a 4.1-fold enhancement and a 2.7-fold decline in the PA_{808}/PA_{1048} and $F^{ex:808}_{em:1550}/F^{ex:980}_{em:1080}$ signals within 2 h, respectively, which allowed the quantification of the H_2O_2 level in early stages of lymphatic metastasis.[95]

https://doi.org/10.1021/acsnano.3c01641
ACS Nano XXXX, XXX, XXX−XXX

Excited metal complexes might encounter an oxygen-induced quenching process in which O_2 molecules can interfere with the normal radiative relaxation of the complexes from their excited triplet state to the ground state, through two competing nonradiative pathways (*i.e.*, charge transfer or noncharge transfer).[185] The mechanism has been employed in the designing of RNPs for directly detecting the concentration of O_2.[186] For instance, an amphiphilic cyclic oligosaccharide, namely, β-cyclodextrin (β-CD), was employed to incorporate bis(2-(2′-benzothienyl)-pyridinato-N,C3′) iridium 4,6-dioxo-heptanoic (Ir-BTPHSA) inside its hydrophobic cavity in a host−guest strategy. In addition, β-CD was further conjugated with Cy7, a well-known O_2-insensitive NIR-I emissive fluorescent dye ($F^{ex:747}_{em:819}$). Ir-BTPHSA was designed such that it contained metalated heterocyclic ligands and an oxygen-donor ligand (4,6-dioxoheptanoic) to improve the QY of the complex ($F^{ex:488}_{em:606}$) and aqueous stability of the dye, respectively. Through this strategy, Xiao *et al.* could protect the heterocycle ligands from the surrounding microenvironment, alleviating the adverse impact of their hydrophobicity on direct O_2 sensing. In addition, the cyclometalated Ir(III) complexes could also provide a salient affinity toward the tumor cells which, in contrast to normal cells, are inherently rich in lipophilic cations, serving as a kind of targeting agent to increase the specificity of the probes toward the tumor cells. In the anoxic conditions, the intensity of the $F^{ex:488}_{em:606}$ signal, which was under suppression by an O_2-induced quenching effect, got rapidly revived and experienced a significant enhancement, while that of the reference NIR-I signal remained constant. The results of *in vitro* and *in vivo* experiments demonstrated that the probe could target the nuclei of LS180 colorectal cancer cells for quantitatively determining the oxygen level as well as mapping the hypoxic condition in the tumor site of intratumorally treated cancer-bearing mice.[187]

4. CONCLUSION

The accurate and comprehensive assessments of the abnormal levels of biomarkers and their potential correlations with one another are of utmost importance not only for timely diagnosing the onset of the diseases but also to provide the physicians with reliable inspection techniques to assess the therapeutic effect of the prescribed medications during the course of treatment. Undeniably, such advances would help scientists take further steps toward translating early diagnosis and individual therapy techniques into widespread clinical practices in order to relieve discomforts and maximize the lifespan of patients. It has been suggested that the detection methodologies affording the ratiometric characteristics are better candidates in order to take part in the realization of these universal desires, compared to the conventional absolute-intensity dependent methods. The long-lasting obsession with the improvement in the performance of the noninvasive diagnostic techniques has been a driving force for researchers in the field to prepare RNPs with the capability of deriving maximized amount of data from *in vivo* microenvironments. Moreover, falsified signals, which might be obtained as the result of inevitable interferences induced by the complex biological systems in *in vivo* signal transduction, highlight the necessity for developing advanced techniques to boost the reliability of the results. Accordingly, the recent and key advances in the design of RNPs with the capabilities of minimizing the falsified signals as well as revealing maximized information from the areas of interest were reviewed. The results of the above-mentioned studies clearly state that deeper insights on the etiological factors involved in the development and progression of diseases can be achieved by means of the advanced RNPs, which in turn might lead to the emergence of better methods or medications for preventing or curing illnesses. We hope that our work provides researchers with further enlightenment and understanding about the current status and challenges of the research area in order to promote further exciting ideas and foster collaboration in the field.

5. CHALLENGES AND FUTURE PERSPECTIVE

Although numerous high-performance RNPs have been successfully developed for visualizing different types of biomarkers of life-threatening diseases, addressing some unmet challenges as well as the necessity of performing further optimizations in the methods or the molecular architecture of the current RNPs might offer plenty of room for improvement.

Ideally, RNPs should be able to provide maximized information from the biological microenvironment, while avoid getting affected by the undesirable interferences induced by their host organisms. As reviewed above, some steps toward achieving the goal have been taken. For instance, dual-modality NIR-II emissive imaging agents were isolated from the interfering substances of the biological microenvironment.[95] It can be expected that the idea of minimizing the affectability of RNPs from their surroundings multifaceted media might be further employed to prepare innovative RNPs with dynamic and reliable responses. We envision that such integrated strategies might have the most potential to be translated to clinical applications, in case that they satisfy the primary requirements such as biosafety and cost-effectiveness.

Although RNPs with a dynamic response are in favor of real-time monitoring of the pathological variations, the cycles of reversibility reported in the corresponding studies are mostly low. This means that after a few cycles of the induced variations in the level of the analyte, the ratiometric signal might not be able to provide reliable information. This might be caused by the perturbation in stability or degradation of the chemical structure in the host microenvironment. Thus, further optimizations in the chemical structures of the corresponding probes might be needed. As implied in the previous paragraph, one feasible approach to prolong the lifespan of the probe might be the encapsulation of the probes with analyte permeable shells to shield the structure from being degraded in the microenvironment.

The recognition units incorporated in the structure of certain RNPs might lack specificity toward the analyte of interest, in some cases. For instance, hydrazide compounds and diphenyl phosphinate, which have been extensively employed as the $ONOO^-$-sensitive moieties in RNPs, can also react with $O_2^{\bullet-}$ and HClO species, respectively.[21,188−190] As another example, although C=C or C=N bond in the structure can be regarded as the recognition sites for hydrogen sulfide, some other entities such as thiols, hydroxyl groups and $ONOO^-$ would also be able to trigger a nucleophilic addition reaction with the bonds.[23] Consequently, the issue might lead to the generation of false positive or negative signals while the corresponding probes are residing in the complex biological systems. Thus, further attempts are expected to be made on introducing "super-exclusive" sets of recognition units to improve the specificity of certain measurements.

The short half-lives of many reactive species have troubled researchers to determine the "benign intracellular concen-

https://doi.org/10.1021/acsnano.3c01641
ACS Nano XXXX, XXX, XXX−XXX

tration" of some of them,[191] which in turn leads to a questionable judgment about the sufficiency of their corresponding sensors' sensitivity. On the other hand, the sensitivity values of some of the developed RNPs for detecting those species with known benign intracellular concentrations do not seem to be sufficient. For instance, it has been reported that during liver injury, the concentration of NO in the liver could get elevated to about 0.5−25 nM, which is 5 times its normal value in the tissue.[101,192] Meanwhile, the limit of detection (LOD) values for most of the reported NO detectors are far beyond the range.[85,104,120] Thus, it seems that extra interdisciplinary efforts should be made to determine the intracellular "safe margin" of the species as well as improving the LOD of their corresponding detectors.

As described above, the lack of sensitivity of NIR-II emissive agents (*e.g.*, QDs, Ln-doped DCNPs, *etc.*) toward the biological entities has made researchers employ certain dye molecules together with the agents to prepare NIR-II emitting RNPs by taking advantage of mechanisms such as IF. However, some potential drawbacks of dyes such as low QY and photostability might have negative impact on the performance of corresponding RNPs. Hence, developing NIR-II emitting agents with the capability of independently affording ratiometric characteristics might offer valuable opportunities for improving the performance of the NIR-II RNPs.

As reviewed above, the majority of constructed RNPs were designed based on the susceptibility of certain chemical groups to undergoing irreversible cleavage or destruction during the sensing process of analytes of interest. The irreversible recognition mechanism prevents the corresponding RNPs from taking part in long-term *in vivo* inspection of the species whose concentrations are spatiotemporally changed in response to microenvironmental stimuli. Therefore, it is expected that providing solutions for overcoming the challenge would further promote researchers' interests.

As it can be inferred from the reviewed studies, fluorescence and photoacoustic modes have exhibited great potential for getting involved in dual-modality ratiometric practices, which as mentioned above might make a valuable contribution to realizing personalized therapy. The relatively similar imaging parameters such as excitation pathways and acquisition time have made these photon-based modalities more technologically compatible compared to other sets of modalities. On the other hand, in addition to chemically engineering the constituents of the corresponding RNPs in order to provide more potent probes, it can be envisioned that the fast-paced technological advancements in other fields of engineering (*e.g.*, mechanical and electronic) might lead to the emergence of instruments with the capability of merging compatible imaging techniques or deriving maximized data during a conventional single-mode ratiometric measurment. For instance, advancements in electronic engineering are constantly contributing to the development of more sensitive photomultiplier tubes, which in turn enables the researchers to visualize the dimmest signals arising from the biological microenvironments, maximizing the obtained data by RNPs.[193]

AUTHOR INFORMATION

Corresponding Author

Mingyuan Gao − *Key Laboratory of Radiation Medicine and Protection, School for Radiological and Interdisciplinary Sciences (RAD-X), Collaborative Innovation Center of Radiation Medicine of Jiangsu Higher Education Institutions, Soochow University, Suzhou 215123, People's Republic of China;* orcid.org/0000-0002-7360-3684; Email: gaomy@suda.edu.cn

Authors

Mohammad Javad Afshari − *Key Laboratory of Radiation Medicine and Protection, School for Radiological and Interdisciplinary Sciences (RAD-X), Collaborative Innovation Center of Radiation Medicine of Jiangsu Higher Education Institutions, Soochow University, Suzhou 215123, People's Republic of China;* orcid.org/0000-0001-5077-570X

Xiaju Cheng − *Key Laboratory of Radiation Medicine and Protection, School for Radiological and Interdisciplinary Sciences (RAD-X), Collaborative Innovation Center of Radiation Medicine of Jiangsu Higher Education Institutions, Soochow University, Suzhou 215123, People's Republic of China*

Guangxin Duan − *Key Laboratory of Radiation Medicine and Protection, School for Radiological and Interdisciplinary Sciences (RAD-X), Collaborative Innovation Center of Radiation Medicine of Jiangsu Higher Education Institutions, Soochow University, Suzhou 215123, People's Republic of China*

Ruixue Duan − *Key Laboratory of Radiation Medicine and Protection, School for Radiological and Interdisciplinary Sciences (RAD-X), Collaborative Innovation Center of Radiation Medicine of Jiangsu Higher Education Institutions, Soochow University, Suzhou 215123, People's Republic of China*

Shuwang Wu − *Key Laboratory of Radiation Medicine and Protection, School for Radiological and Interdisciplinary Sciences (RAD-X), Collaborative Innovation Center of Radiation Medicine of Jiangsu Higher Education Institutions, Soochow University, Suzhou 215123, People's Republic of China*

Jianfeng Zeng − *Key Laboratory of Radiation Medicine and Protection, School for Radiological and Interdisciplinary Sciences (RAD-X), Collaborative Innovation Center of Radiation Medicine of Jiangsu Higher Education Institutions, Soochow University, Suzhou 215123, People's Republic of China;* orcid.org/0000-0001-7654-8724

Zi Gu − *School of Chemical Engineering and Australian Centre for NanoMedicine (ACN), University of New South Wales, Sydney, New South Wales 2052, Australia;* orcid.org/0000-0002-7153-6596

Complete contact information is available at: https://pubs.acs.org/10.1021/acsnano.3c01641

Author Contributions

[#]M.J.A. and X.C. contributed equally.

Notes

The authors declare no competing financial interest.

ACKNOWLEDGMENTS

The authors are grateful to the financial support from the National Key Research and Development Program of China (2018YFA0208800), the National Natural Science Foundation of China (81720108024, 82130059, 82222033, 82172003) and Priority Academic Program Development of Jiangsu Higher Education Institutions (PAPD).

https://doi.org/10.1021/acsnano.3c01641
ACS Nano XXXX, XXX, XXX−XXX

VOCABULARY

Disease-associated physiological hallmarks, are those physiological characteristics that are known as the indicators of onset or progression of the diseases. Noninvasive detection of the bioindicators at the molecular level is of paramount importance for realizing the early diagnosis of the diseases; Ratiometric nanoprobes (RNPs), are a category of smart diagnostic probes that can provide their outputs in two separate channels. This enables the researchers to employ the information provided in one of the channels as the reference and the other one as the detecting indicator; Spatiotemporal heterogeneity, is defined as the time- and space-dependent variations in the level of biomarkers in the lesion area. This might be caused by the dynamic interactions of the biological entities with each other or as the result of certain physiological processes; Self-illuminating probes, can emit light without the necessity of real-time external excitation such as laser light. They can eliminate the autofluorescence phenomenon and minimize the photobleaching effect; Förster resonance energy transfer (FRET), is a mechanism with which the energy is transferred from one fluorophore (donor) to another adjacent fluorophore (acceptor) that has satisfactory quantum yield and spectral overlap with the donor; Internal charge transfer (ICT), is a mechanism that enables the transfer of electron from an electron-donating group to an electron-deficient moiety within a molecule; Inner filtration (IF) effect, refers to the phenomenon in which the energy that has been supposed to radiatively release from a fluorescent molecule is absorbed by a quencher in the vicinity of the molecule

REFERENCES

(1) Yin, L.; Sun, H.; Zhang, H.; He, L.; Qiu, L.; Lin, J.; Xia, H.; Zhang, Y.; Ji, S.; Shi, H.; Gao, M. Quantitatively Visualizing Tumor-Related Protease Activity in Vivo Using a Ratiometric Photoacoustic Probe. *J. Am. Chem. Soc.* **2019**, *141*, 3265−3273.

(2) Page-McCaw, A.; Ewald, A. J.; Werb, Z. Matrix Metalloproteinases and the Regulation of Tissue Remodelling. *Nat. Rev. Mol. Cell Biol.* **2007**, *8*, 221−233.

(3) DeLeon-Pennell, K. Y.; Meschiari, C. A.; Jung, M.; Lindsey, M. L. Matrix Metalloproteinases in Myocardial Infarction and Heart Failure. *Prog. Mol. Biol. Transl. Sci.* **2017**, *147*, 75−100.

(4) Zhang, X.; Huang, S.; Guo, J.; Zhou, L.; You, L.; Zhang, T.; Zhao, Y. Insights into the Distinct Roles of MMP-11 in Tumor Biology and Future Therapeutics (Review). *Int. J. Oncol.* **2016**, *48*, 1783−1793.

(5) Shyamala, K.; Girish, H. C.; Murgod, S. Risk of Tumor Cell Seeding through Biopsy and Aspiration Cytology. *J. Int. Soc. Prev. Community Dent.* **2014**, *4*, 5−11.

(6) Marusyk, A.; Almendro, V.; Polyak, K. Intra-Tumour Heterogeneity: A Looking Glass for Cancer? *Nat. Rev. Cancer* **2012**, *12*, 323−334.

(7) Ma, T.; Hou, Y.; Zeng, J.; Liu, C.; Zhang, P.; Jing, L.; Shangguan, D.; Gao, M. Dual-Ratiometric Target-Triggered Fluorescent Probe for Simultaneous Quantitative Visualization of Tumor Microenvironment Protease Activity and pH In Vivo. *J. Am. Chem. Soc.* **2018**, *140*, 211−218.

(8) Yoon, S.; Cheon, S. Y.; Park, S.; Lee, D.; Lee, Y.; Han, S.; Kim, M.; Koo, H. Recent Advances in Optical Imaging through Deep Tissue: Imaging Probes and Techniques. *Biomater. Res.* **2022**, *26*, 57−83.

(9) Ding, F.; Fan, Y.; Sun, Y.; Zhang, F. Beyond 1000 nm Emission Wavelength: Recent Advances in Organic and Inorganic Emitters for Deep-Tissue Molecular Imaging. *Adv. Healthc. Mater.* **2019**, *8*, 1900260−1900274.

(10) Genicio, N.; Bañobre-López, M.; Gröhn, O.; Gallo, J. Ratiometric Magnetic Resonance Imaging: Contrast Agent Design Towards Better Specificity and Quantification. *Coord. Chem. Rev.* **2021**, *447*, 214150−214164.

(11) Jing, L.; Yang, C.; Zhang, P.; Zeng, J.; Li, Z.; Gao, M. Nanoparticles Weaponized with Built-In Functions for Imaging-Guided Cancer Therapy. *VIEW* **2020**, *1*, 19−33.

(12) Tapeinos, C.; Larrañaga, A.; Tomatis, F.; Bizeau, J.; Marino, A.; Battaglini, M.; Pandit, A.; Ciofani, G. Advanced Functional Materials and Cell-Based Therapies for the Treatment of Ischemic Stroke and Postischemic Stroke Effects. *Adv. Funct. Mater.* **2020**, *30*, 1906283−1906304.

(13) Blanco, E.; Shen, H.; Ferrari, M. Principles of Nanoparticle Design for Overcoming Biological Barriers to Drug Delivery. *Nat. Biotechnol.* **2015**, *33*, 941−951.

(14) Han, Y.; Wang, T.; Liu, H.; Zhang, S.; Zhang, H.; Li, M.; Sun, Q.; Li, Z. The Release and Detection of Copper Ions from Ultrasmall Theranostic Cu_{2-X}se Nanoparticles. *Nanoscale* **2019**, *11*, 11819−11829.

(15) Xu, Y.; Zhang, P.; Gao, A.; Xu, R.; Wang, Z.; Shen, Q.; Zhao, Z.; Meng, L.; Dang, D. Recent Advances in Activatable NIR-II Organic Fluorophores for Biomedical Applications. *Mater. Chem. Front.* **2023**, *7*, 828−845.

(16) Miao, Q.; Pu, K. Emerging Designs of Activatable Photoacoustic Probes for Molecular Imaging. *Bioconjugate Chem.* **2016**, *27*, 2808−2823.

(17) Salaam, J.; Minoshima, M.; Kikuchi, K. Recent Advances in Activatable ^{19}F Magnetic Resonance Imaging Nano-Probes for the Detection of Biomarkers. *Analysis Sensing* **2022**, *n/a*, 202200081−202200097.

(18) Ma, T.; Zhang, P.; Hou, Y.; Ning, H.; Wang, Z.; Huang, J.; Gao, M. ″Smart″ Nanoprobes for Visualization of Tumor Microenvironments. *Adv. Healthcare Mater.* **2018**, *7*, 1800391−1800407.

(19) Huang, X.; Song, J.; Yung, B. C.; Huang, X.; Xiong, Y.; Chen, X. Ratiometric Optical Nanoprobes Enable Accurate Molecular Detection and Imaging. *Chem. Soc. Rev.* **2018**, *47*, 2873−2920.

(20) Huang, H.; Qiu, R.; Yang, H.; Ren, F.; Wu, F.; Zhang, Y.; Zhang, H.; Li, C. Advanced NIR Ratiometric Probes for Intravital Biomedical Imaging. *Biomed. Mater.* **2022**, *17*, 14107−14125.

(21) Zhao, C.; Chen, J.; Zhong, R.; Chen, D. S.; Shi, J.; Song, J. Oxidative-Species-Selective Materials for Diagnostic and Therapeutic Applications. *Angew. Chem., Int. Ed.* **2021**, *60*, 9804−9827.

(22) Zhang, C.; Wang, X.; Du, J.; Gu, Z.; Zhao, Y. Reactive Oxygen Species-Regulating Strategies Based on Nanomaterials for Disease Treatment. *Adv. Sci.* **2021**, *8*, 2002797−2002830.

(23) Ma, Q.; Xu, S.; Zhai, Z.; Wang, K.; Liu, X.; Xiao, H.; Zhuo, S.; Liu, Y. Recent Progress of Small-Molecule Ratiometric Fluorescent Probes for Peroxynitrite in Biological Systems. *Chem. Eur. J.* **2022**, *28*, 202200828−202200841.

(24) Shao, J.; Sun, S.; Zhan, D.; Pan, L.; Min, G.; Li, X.; Huang, K.; Chen, W.; Yang, L.; Liu, X.-Y.; Lin, N. Phycocyanin - Carbon Dots Nanoprobe for the Ratiometric Fluorescence Determination of Peroxynitrite. *Spectrochim. Acta, Part A* **2022**, *275*, 121177−121184.

(25) Li, Z.; Lu, J.; Pang, Q.; You, J. Construction of a Near-Infrared Fluorescent Probe for Ratiometric Imaging of Peroxynitrite During Tumor Progression. *Analyst* **2021**, *146*, 5204−5211.

(26) Lin, X.; Liu, W.; Xu, S.; Li, Z.; Zhang, H.; Yu, M. Imaging of Intracellular Bisulfate Based on Sensitive Ratiometric Fluorescent Probes. *Spectrochim. Acta, Part A* **2022**, *265*, 120335−120341.

(27) Zhang, C.; Li, J.; Chen, X.; Hu, Y.; Huang, X. Rational Design of Ratiometric Fluorescent Probes for Bisulfite and Viscosity Detection in Mitochondria without Spectral Crosstalk. *Dyes Pigm.* **2022**, *207*, 110666−110673.

(28) Li, D.-P.; Tang, F.; Wen, K.; Yang, Z.; Xiao, H.; Zhou, Z. A Ratiometric Fluorescent Probe for SO_2 Derivatives Based on a New Coumarin-Hemicyanine Dye in Living Cells. *Microchem. J.* **2022**, *175*, 107233−107238.

(29) Yang, X.; Yang, Y.; Zhou, T.; Jin, M.; Jing, X.; Miao, C. h.; Li, W. A Mitochondria-Targeted Ratiometric Fluorescent Probe for

https://doi.org/10.1021/acsnano.3c01641
ACS Nano XXXX, XXX, XXX−XXX

Detection of SO_2 Derivatives in Living Cells and In Vivo. *J. Photochem. Photobiol., A* **2019**, *372*, 212−217.
(30) Li, Z.; Zhang, Y.; Jiang, Y.; Li, H.; Chen, C.; Liu, W. A Ratiometric Fluorescent Probe Based on Two-Isophorone Fluorophore for Detecting Cysteine. *J. Mater. Chem. B* **2022**, *10*, 6207−6213.
(31) Wang, L.; Niu, K.; Chen, S.; Wu, Y.; Tang, Y.; Hou, S.; Wu, W. Near-Infrared Fluorescent Probe with a Self-Immolative Spacer for Ratiometric Imaging Alkaline Phosphatase in Cell and Zebrafish. *Dyes Pigm.* **2023**, *209*, 110910−110916.
(32) Han, S.; Zhang, H.; Yue, X.; Wang, J.; Yang, L.; Wang, B.; Song, X. A Ratiometric, Fast-Responsive, and Single-Wavelength Excited Fluorescent Probe for the Discrimination of Cys and Hcy. *Anal. Chem.* **2021**, *93*, 10934−10939.
(33) Luo, X.; Wang, R.; Lv, C.; Chen, G.; You, J.; Yu, F. Detection of Selenocysteine with a Ratiometric Near-Infrared Fluorescent Probe in Cells and in Mice Thyroid Diseases Model. *Anal. Chem.* **2020**, *92*, 1589−1597.
(34) Park, S.-H.; Kwon, N.; Lee, J.-H.; Yoon, J.; Shin, I. Synthetic Ratiometric Fluorescent Probes for Detection of Ions. *Chem. Soc. Rev.* **2020**, *49*, 143−179.
(35) Lee, M. H.; Kim, J. S.; Sessler, J. L. Small Molecule-Based Ratiometric Fluorescence Probes for Cations, Anions, and Biomolecules. *Chem. Soc. Rev.* **2015**, *44*, 4185−4191.
(36) Jin, H.; Yang, M.; Sun, Z.; Gui, R. Ratiometric Two-Photon Fluorescence Probes for Sensing, Imaging and Biomedicine Applications at Living Cell and Small Animal Levels. *Coord. Chem. Rev.* **2021**, *446*, 214114−214155.
(37) Jin, H.; Jiang, X.; Sun, Z.; Gui, R. Phosphorescence-Based Ratiometric Probes: Design, Preparation and Applications in Sensing, Imaging and Biomedicine Therapy. *Coord. Chem. Rev.* **2021**, *431*, 213694−213732.
(38) Fang, H.; Wang, C.; Chen, Y.; Chen, Z.; Yao, S.; Yang, S.; Dong, L.; Guo, Z.; He, W. A Photoacoustic Zn^{2+} Sensor Based on a Merocyanine/Xanthene-6-Ol Hybrid Chromophore and Its Ratiometric Imaging in Mice. *Inorg. Chem. Front.* **2021**, *8*, 3402−3410.
(39) Sperling, R. A.; Aisen, P. S.; Beckett, L. A.; Bennett, D. A.; Craft, S.; Fagan, A. M.; Iwatsubo, T.; Jack, C. R.; Kaye, J.; Montine, T. J.; Park, D. C.; Reiman, E. M.; Rowe, C. C.; Siemers, E.; Stern, Y.; Yaffe, K.; Carrillo, M. C.; Thies, B.; Morrison-Bogorad, M.; Wagster, M. V.; Phelps, C. H. Toward Defining the Preclinical Stages of Alzheimer's Disease: Recommendations from the National Institute on Aging-Alzheimer's Association Workgroups on Diagnostic Guidelines for Alzheimer's Disease. *Alzheimer's Dementia* **2011**, *7*, 280−292.
(40) Zhang, Q.; Hu, X.; Dai, X.; Ling, P.; Sun, J.; Chen, H.; Gao, F. General Strategy to Achieve Color-Tunable Ratiometric Two-Photon Integrated Single Semiconducting Polymer Dot for Imaging Hypochlorous Acid. *ACS Nano* **2021**, *15*, 13633−13645.
(41) Chen, H.; Zhang, H.; Wang, Z. A Ratiometric Fluorescent Probe Based on Peptide Modified $MnFe_2O_4$ Nanoparticles for Matrix Metalloproteinase-7 Activity Detection In Vitro and In Vivo. *Analyst* **2022**, *147*, 1581−1588.
(42) Shen, W.; Xu, H.; Feng, J.; Sun, W.; Hu, G.; Hu, Y.; Yang, W. A Ratiometric and Colorimetric Fluorescent Probe Designed Based on FRET for Detecting SO_3^{2-}/HSO_3^- in Living Cells and Mice. *Spectrochim. Acta, Part A* **2021**, *263*, 120183−120191.
(43) Liu, H.-W.; Zhang, H.; Lou, X.; Teng, L.; Yuan, J.; Yuan, L.; Zhang, X.-B.; Tan, W. Imaging of Peroxynitrite in Drug-Induced Acute Kidney Injury with a Near-Infrared Fluorescence and Photoacoustic Dual-Modal Molecular Probe. *Chem. Commun.* **2020**, *56*, 8103−8106.
(44) Zhang, T.; Li, L.; Huo, F.; Zhang, W.; Chao, J.; Yin, C. Alkyl Chain Regulated Cytomembrane and Mitochondria Targeting Fluorescent Probes for Ratiometric Sensing SO_2 and Its Bio-Application in Mice Model. *Sens. Actuators, B* **2021**, *342*, 130041−130047.
(45) Jing, X.; Yu, F.; Lin, W. Monitoring Cysteine Level Changes under LPS or H_2O_2 Induced Oxidative Stress Using a Polymer-Based Ratiometric Fluorescent Probe. *Anal. Chim. Acta* **2021**, *1174*, 338738−338745.
(46) Huang, L.; Su, W.; Zhao, Y.; Zhan, J.; Lin, W. Synthesis, Molecular Docking Calculation, Fluorescence and Bioimaging of Mitochondria-Targeted Ratiometric Fluorescent Probes for Sensing Hypochlorite In Vivo. *J. Mater. Chem. B* **2021**, *9*, 2666−2673.
(47) Jia, P.; Zhuang, Z.; Liu, C.; Wang, Z.; Duan, Q.; Li, Z.; Zhu, H.; Zhang, F.; Sheng, W.; Zhu, B. Development of a Ratiometric Fluorescent Probe with a Large Emission Shift for Imaging $ONOO^-$ in Live Cells and Zebrafish. *Dyes Pigm.* **2020**, *173*, 107942−107946.
(48) Wang, L.; Chen, S.; Ma, X.; Wu, Y.; Tang, Y.; Hou, S. Fast and Sensitive Near-Infrared Ratiometric Fluorescent Probe with a Self-Immolative Spacer for Imaging of Endogenous Alkaline Phosphatase Activity in Cells and In Vivo. *Talanta* **2022**, *249*, 123658−123665.
(49) Liu, Y.; Nie, J.; Niu, J.; Wang, W.; Lin, W. An AIE + ESIPT Ratiometric Fluorescent Probe for Monitoring Sulfur Dioxide with Distinct Ratiometric Fluorescence Signals in Mammalian Cells, Mouse Embryonic Fibroblast and Zebrafish. *J. Mater. Chem. B* **2018**, *6*, 1973−1983.
(50) Zhou, D.-Y.; Ou-Yang, J.; Li, Y.; Jiang, W.-L.; Tian, Y.; Yi, Z.-M.; Li, C.-Y. A Ratiometric Fluorescent Probe for the Detection of Peroxynitrite with Simple Synthesis and Large Emission Shift and Its Application in Cells Image. *Dyes Pigm.* **2019**, *161*, 288−295.
(51) Huang, Y.; Zhang, Y.; Huo, F.; Chao, J.; Yin, C. A near-Infrared Ratiometric Fluorescent Probe with Large Stokes Based on Isophorone for Rapid Detection of ClO^- and Its Bioimaging in Cell and Mice. *Sens. Actuators, B* **2019**, *287*, 453−458.
(52) Lan, J.-S.; Zeng, R.-F.; Ding, Y.; Zhang, Y.; Zhang, T.; Wu, T. A Simple Pyrene-Hemicyanine Fluorescent Probe for Colorimetric and Ratiometric Detection of SO_2 Derivatives in the Mitochondria of Living Cells and Zebrafish In Vivo. *Sens. Actuators, B* **2018**, *268*, 328−337.
(53) Li, C.; Chen, G.; Zhang, Y.; Wu, F.; Wang, Q. Advanced Fluorescence Imaging Technology in the Near-Infrared-II Window for Biomedical Applications. *J. Am. Chem. Soc.* **2020**, *142*, 14789−14804.
(54) Jiang, Y.; Upputuri, P. K.; Xie, C.; Lyu, Y.; Zhang, L.; Xiong, Q.; Pramanik, M.; Pu, K. Broadband Absorbing Semiconducting Polymer Nanoparticles for Photoacoustic Imaging in Second Near-Infrared Window. *Nano Lett.* **2017**, *17*, 4964−4969.
(55) Hong, G.; Antaris, A. L.; Dai, H. Near-Infrared Fluorophores for Biomedical Imaging. *Nat. Biomed. Eng.* **2017**, *1*, 10−31.
(56) Zhang, X.; Jiang, K.; Jiang, S.; Zhao, F.; Chen, P.; Huang, P.; Lin, J. In Vivo Near-Infrared Fluorescence/Ratiometric Photoacoustic Duplex Imaging of Lung Cancer-Specific Hnqo1. *Anal. Chem.* **2022**, *94*, 13770−13776.
(57) Wen, L.; Ma, X.; Yang, J.; Jiang, M.; Peng, C.; Ma, Z.; Yu, H.; Li, Y. A New Ratiometric Design Strategy Based on Modulation of π-Conjugation Unit for Developing Fluorescent Probe and Imaging of Cellular Peroxynitrite. *Anal. Chem.* **2022**, *94*, 4763−4769.
(58) Wu, R.; Chen, Z.; Huo, H.; Chen, L.; Su, L.; Zhang, X.; Wu, Y.; Yao, Z.; Xiao, S.; Du, W.; Song, J. Ratiometric Detection of H_2S in Liver Injury by Activated Two-Wavelength Photoacoustic Imaging. *Anal. Chem.* **2022**, *94*, 10797−10804.
(59) Fan, X.-P.; Yang, W.; Ren, T.-B.; Xu, S.; Gong, X.-Y.; Zhang, X.-B.; Yuan, L. Engineering a Ratiometric Photoacoustic Probe with a Hepatocyte-Specific Targeting Ability for Liver Injury Imaging. *Anal. Chem.* **2022**, *94*, 1474−1481.
(60) Shangguan, L.; Wang, J.; Qian, X.; Wu, Y.; Liu, Y. Mitochondria-Targeted Ratiometric Chemdosimeter to Detect Hypochlorite Acid for Monitoring the Drug-Damaged Liver and Kidney. *Anal. Chem.* **2022**, *94*, 11881−11888.
(61) Shi, Y.; Huo, F.; Yue, Y.; Yin, C. N-Positive Ion Activated Rapid Addition and Mitochondrial Targeting Ratiometric Fluorescent Probes for In Vivo Cell H_2S Imaging. *Front. Chem. Sci. Eng.* **2022**, *16*, 64−71.
(62) Ren, H.; Huo, F.; Wen, W.; Yin, C. Engineering an ESIPT-Based Fluorescent Probe for Dual-Channel (Vis/NIR) Ratiometric

https://doi.org/10.1021/acsnano.3c01641
ACS Nano XXXX, XXX, XXX−XXX

Monitoring of Intracellular Sulfur Dioxide by Single Wavelength Excitation. *Dyes Pigm.* **2022**, *199*, 110111−110115.
(63) Chang, D.; Zhao, Z.; Li, W.; Shi, H.; Yang, Y.; Shi, L.; Shuang, S. Hg^{2+}-Mediated Ratiometric Fluorescent Carbon Dots for Imaging Glutathione in Living Cells and Zebrafish. *ACS Sustainable Chem. Eng.* **2022**, *10*, 10068−10076.
(64) Ma, Y.; Guo, B.; Ge, J.-Y.; Chen, L.; Lv, N.; Wu, X.; Chen, J.; Chen, Z. Rational Design of a Near-Infrared Ratiometric Probe with a Large Stokes Shift: Visualization of Polarity Abnormalities in Non-Alcoholic Fatty Liver Model Mice. *Anal. Chem.* **2022**, *94*, 12383−12390.
(65) Zeng, W.; Wu, L.; Sun, Y.; Wang, Y.; Wang, J.; Ye, D. Ratiometric Imaging of MMP-2 Activity Facilitates Tumor Detection Using Activatable Near-Infrared Fluorescent Semiconducting Polymer Nanoparticles. *Small* **2021**, *17*, 2101924−2101936.
(66) Brown, J. M.; Wilson, W. R. Exploiting Tumour Hypoxia in Cancer Treatment. *Nat. Rev. Cancer* **2004**, *4*, 437−447.
(67) He, Z.; Chou, Y.; Zhou, H.; Zhang, H.; Cheng, T.; Liu, G. A Nitroreductase and Acidity Detecting Dual Functional Ratiometric Fluorescent Probe for Selectively Imaging Tumor Cells. *Org. Biomol. Chem.* **2018**, *16*, 3266−3272.
(68) Zhang, Z.; Feng, Q.; Yang, M.; Tang, Y. A Ratiometric Fluorescent Biosensor Based on Conjugated Polymers for Sensitive Detection of Nitroreductase and Hypoxia Diagnosis in Tumor Cells. *Sens. Actuators, B* **2020**, *318*, 128257−128264.
(69) Sarkar, S.; Lee, H.; Ryu, H. G.; Singha, S.; Lee, Y. M.; Reo, Y. J.; Jun, Y. W.; Kim, K. H.; Kim, W. J.; Ahn, K. H. A Study on Hypoxia Susceptibility of Organ Tissues by Fluorescence Imaging with a Ratiometric Nitroreductase Probe. *ACS Sens.* **2021**, *6*, 148−155.
(70) Zhu, D.; Xue, L.; Li, G.; Jiang, H. A Highly Sensitive Near-Infrared Ratiometric Fluorescent Probe for Detecting Nitroreductase and Cellular Imaging. *Sens. Actuators, B* **2016**, *222*, 419−424.
(71) Lan, Q.; Yu, P.; Yan, K.; Li, X.; Zhang, F.; Lei, Z. Polymethine Molecular Platform for Ratiometric Fluorescent Probes in the Second Near-Infrared Window. *J. Am. Chem. Soc.* **2022**, *144*, 21010−21015.
(72) Xu, J.-Q.; Gao, M.-J.; Guo, J.-S.; Wang, Y.-H.; Wei, R.; Meng, Y.-L.; Kang, Y.-F. A Highly Selective Probe for Ratiometric Imaging Peroxynitrite in Living Cells and In Vivo. *Bioorg. Chem.* **2022**, *128*, 106055−106061.
(73) Wu, L.; Wang, Y.; Weber, M.; Liu, L.; Sedgwick, A. C.; Bull, S. D.; Huang, C.; James, T. D. ESIPT-Based Ratiometric Fluorescence Probe for the Intracellular Imaging of Peroxynitrite. *Chem. Commun.* **2018**, *54*, 9953−9956.
(74) Li, Q.; Yang, Z. A Boronate-Based Ratiometric Fluorescent Probe for Fast Selective Detection of Peroxynitrite. *Tetrahedron Lett.* **2018**, *59*, 125−129.
(75) Nazha, B.; Moussaly, E.; Zaarour, M.; Weerasinghe, C.; Azab, B. Hypoalbuminemia in Colorectal Cancer Prognosis: Nutritional Marker or Inflammatory Surrogate? *World J. Gastrointest. Surg.* **2015**, *7*, 370−377.
(76) Merlot, A. M.; Kalinowski, D. S.; Richardson, D. R. Unraveling the Mysteries of Serum Albumin—More Than Just a Serum Protein. *Front. Physiol.* **2014**, *5*, 299−305.
(77) Zhang, Z.; Achilefu, S. Design, Synthesis and Evaluation of Near-Infrared Fluorescent pH Indicators in a Physiologically Relevant Range. *Chem. Commun.* **2005**, 5887−5889.
(78) Usama, S. M.; Caldwell, D. R.; Shrestha, P.; Luciano, M. P.; Patel, N. L.; Kalen, J. D.; Ivanic, J.; Schnermann, M. J. Modified Norcyanines Enable Ratiometric pH Imaging Beyond 1000 nm. *Biosens. Bioelectron.* **2022**, *217*, 114610−114616.
(79) Lin, P.; Chen, D.; Zhang, L.; Xu, J.; Huang, Y.; Zhao, S. Near-Infrared Dual-Emission Ratiometric Fluorescence Imaging Nanoprobe for Real-Time Tracing the Generation of Endogenous Peroxynitrite in Single Living Cells and In Vivo. *ACS Omega* **2020**, *5*, 13278−13286.
(80) Huang, H.; Sun, Z.; Yang, H.; Yang, X.; Wu, F.; Sun, Y.; Li, C.; Tian, M.; Zhang, H.; Wang, Q. Precise Examination of Peripheral Vascular Disease for Diabetics with a Novel Multiplexed NIR-II Fluorescence Imaging Technology. *Nano Today* **2022**, *43*, 101378−101385.
(81) Deng, Z.; Bi, S.; Jiang, M.; Zeng, S. Endogenous H_2S-Activated Orthogonal Second Near-Infrared Emissive Nanoprobe for In Situ Ratiometric Fluorescence Imaging of Metformin-Induced Liver Injury. *ACS Nano* **2021**, *15*, 3201−3211.
(82) Sun, Z.; Huang, H.; Zhang, R.; Yang, X.; Yang, H.; Li, C.; Zhang, Y.; Wang, Q. Activatable Rare Earth Near-Infrared-II Fluorescence Ratiometric Nanoprobes. *Nano Lett.* **2021**, *21*, 6576−6583.
(83) Wang, S.; Liu, L.; Fan, Y.; El-Toni, A. M.; Alhoshan, M. S.; li, D.; Zhang, F. In Vivo High-Resolution Ratiometric Fluorescence Imaging of Inflammation Using NIR-II Nanoprobes with 1550 nm Emission. *Nano Lett.* **2019**, *19*, 2418−2427.
(84) Wang, C.; Lin, H.; Ge, X.; Mu, J.; Su, L.; Zhang, X.; Niu, M.; Yang, H.; Song, J. Dye-Sensitized Downconversion Nanoprobes with Emission Beyond 1500 nm for Ratiometric Visualization of Cancer Redox State. *Adv. Funct. Mater.* **2021**, *31*, 2009942−2009952.
(85) Bai, F.; Du, W.; Liu, X.; Su, L.; Li, Z.; Chen, T.; Ge, X.; Li, Q.; Yang, H.; Song, J. A NO-Responsive Ratiometric Fluorescent Nanoprobe for Monitoring Drug-Induced Liver Injury in the Second Near-Infrared Window. *Anal. Chem.* **2021**, *93*, 15279−15287.
(86) Zhang, M.; Wang, Z.; Wang, C.; Wu, Y.; Li, Z.; Liu, Z. Visualizing Oxidative Stress Level for Timely Assessment of Ischemic Stroke via a Ratiometric Near-Infrared-II Luminescent Nanoprobe. *ACS Nano* **2021**, *15*, 11940−11952.
(87) Naczynski, D. J.; Tan, M. C.; Zevon, M.; Wall, B.; Kohl, J.; Kulesa, A.; Chen, S.; Roth, C. M.; Riman, R. E.; Moghe, P. V. Rare-Earth-Doped Biological Composites as In Vivo Shortwave Infrared Reporters. *Nat. Commun.* **2013**, *4*, 2199−2208.
(88) Li, S.; Ma, Q.; Wang, C.; Yang, K.; Hong, Z.; Chen, Q.; Song, J.; Song, X.; Yang, H. Near-Infrared II Gold Nanocluster Assemblies with Improved Luminescence and Biofate for In Vivo Ratiometric Imaging of H_2S. *Anal. Chem.* **2022**, *94*, 2641−2647.
(89) Wang, C.; Niu, M.; Wang, W.; Su, L.; Feng, H.; Lin, H.; Ge, X.; Wu, R.; Li, Q.; Liu, J.; Yang, H.; Song, J. In Situ Activatable Ratiometric NIR-II Fluorescence Nanoprobe for Quantitative Detection of H_2S in Colon Cancer. *Anal. Chem.* **2021**, *93*, 9356−9363.
(90) Ge, X.; Lou, Y.; Su, L.; Chen, B.; Guo, Z.; Gao, S.; Zhang, W.; Chen, T.; Song, J.; Yang, H. Single Wavelength Laser Excitation Ratiometric NIR-II Fluorescent Probe for Molecule Imaging In Vivo. *Anal. Chem.* **2020**, *92*, 6111−6120.
(91) Cao, C.; Zhou, X.; Xue, M.; Han, C.; Feng, W.; Li, F. Dual Near-Infrared-Emissive Luminescent Nanoprobes for Ratiometric Luminescent Monitoring of ClO^- in Living Organisms. *ACS Appl. Mater. Interfaces* **2019**, *11*, 15298−15305.
(92) Liao, N.; Su, L.; Zheng, Y.; Zhao, B.; Wu, M.; Zhang, D.; Yang, H.; Liu, X.; Song, J. In Vivo Tracking of Cell Viability for Adoptive Natural Killer Cell-Based Immunotherapy by Ratiometric NIR-II Fluorescence Imaging. *Angew. Chem., Int. Ed.* **2021**, *60*, 20888−20896.
(93) Liu, L.; Li, X.; Zhang, H.; Chen, H.; Abualrejal, M. M. A.; Song, D.; Wang, Z. Six-in-One Peptide Functionalized Upconversion@Polydopamine Nanoparticle-Based Ratiometric Fluorescence Sensing Platform for Real-Time Evaluating Anticancer Efficacy through Monitoring Caspase-3 Activity. *Sens. Actuators, B* **2021**, *333*, 129554−129561.
(94) Pei, P.; Hu, H.; Chen, Y.; Wang, S.; Chen, J.; Ming, J.; Yang, Y.; Sun, C.; Zhao, S.; Zhang, F. NIR-II Ratiometric Lanthanide-Dye Hybrid Nanoprobes Doped Bioscaffolds for In Situ Bone Repair Monitoring. *Nano Lett.* **2022**, *22*, 783−791.
(95) Chen, T.; Chen, Z.; Zhou, Q.; Ding, H.; Gong, P.; Wang, J.; Cai, H.; Ao, R.; Yu, M.; Song, J.; Lin, L.; Yang, H. Microenvironment-Tailored Catalytic Nanoprobe for Ratiometric NIR-II Fluorescence/Photoacoustic Imaging of H_2O_2 in Tumor and Lymphatic Metastasis. *Adv. Funct. Mater.* **2022**, *32*, 2208720−2208729.
(96) Shuhendler, A. J.; Pu, K.; Cui, L.; Uetrecht, J. P.; Rao, J. Real-Time Imaging of Oxidative and Nitrosative Stress in the Liver of Live

https://doi.org/10.1021/acsnano.3c01641
ACS Nano XXXX, XXX, XXX−XXX

Animals for Drug-Toxicity Testing. *Nat. Biotechnol.* **2014**, *32*, 373−380.
(97) Jiang, W.-L.; Li, Y.; Wang, W.-X.; Zhao, Y.-T.; Fei, J.; Li, C.-Y. A Hepatocyte-Targeting Near-Infrared Ratiometric Fluorescent Probe for Monitoring Peroxynitrite During Drug-Induced Hepatotoxicity and Its Remediation. *Chem. Commun.* **2019**, *55*, 14307−14310.
(98) Nishio, E.; Watanabe, Y. Glucose-Induced Down-Regulation of NO Production and Inducible NOS Expression in Cultured Rat Aortic Vascular Smooth Muscle Cells: Role of Protein Kinase C. *Biochem. Biophys. Res. Commun.* **1996**, *229*, 857−863.
(99) Gardner, C. R.; Heck, D. E.; Yang, C. S.; Thomas, P. E.; Zhang, X. J.; DeGeorge, G. L.; Laskin, J. D.; Laskin, D. L. Role of Nitric Oxide in Acetaminophen-Induced Hepatotoxicity in the Rat. *Hepatol.* **1998**, *27*, 748−754.
(100) Tang, Y.; Li, Y.; Wang, Z.; Pei, F.; Hu, X.; Ji, Y.; Li, X.; Zhao, H.; Hu, W.; Lu, X.; Fan, Q.; Huang, W. Organic Semiconducting Nanoprobe with Redox-Activatable NIR-II Fluorescence for In Vivo Real-Time Monitoring of Drug Toxicity. *Chem. Commun.* **2019**, *55*, 27−30.
(101) Chen, J. B.; Zhang, H. X.; Guo, X. F.; Wang, H.; Zhang, H. S. Boron-Chelating Fluorescent Probe (Bopb) in the Red Region Combined with CE-LIF for the Detection of NO in Mice Liver. *Electrophoresis* **2016**, *37*, 609−615.
(102) Wang, F.; Yu, S.; Xu, Z.; Li, L.; Dang, Y.; Xu, X.; Luo, Y.; Cheng, Z.; Yu, H.; Zhang, W.; Zhang, A.; Ding, C. Acid-Promoted D-a-D Type Far-Red Fluorescent Probe with High Photostability for Lysosomal Nitric Oxide Imaging. *Anal. Chem.* **2018**, *90*, 7953−7962.
(103) Wang, N.; Yu, X.; Zhang, K.; Mirkin, C. A.; Li, J. Upconversion Nanoprobes for the Ratiometric Luminescent Sensing of Nitric Oxide. *J. Am. Chem. Soc.* **2017**, *139*, 12354−12357.
(104) Reinhardt, C. J.; Zhou, E. Y.; Jorgensen, M. D.; Partipilo, G.; Chan, J. A Ratiometric Acoustogenic Probe for In Vivo Imaging of Endogenous Nitric Oxide. *J. Am. Chem. Soc.* **2018**, *140*, 1011−1018.
(105) Moskowitz, M. A.; Lo, E. H.; Iadecola, C. The Science of Stroke: Mechanisms in Search of Treatments. *Neuron* **2010**, *67*, 181−198.
(106) Cade, W. T. Diabetes-Related Microvascular and Macrovascular Diseases in the Physical Therapy Setting. *Phys. Ther.* **2008**, *88*, 1322−1335.
(107) Pacher, P.; Beckman, J. S.; Liaudet, L. Nitric Oxide and Peroxynitrite in Health and Disease. *Physiol. Rev.* **2007**, *87*, 315−424.
(108) Yin, C.; Zhu, H.; Xie, C.; Zhang, L.; Chen, P.; Fan, Q.; Huang, W.; Pu, K. Organic Nanoprobe Cocktails for Multilocal and Multicolor Fluorescence Imaging of Reactive Oxygen Species. *Adv. Funct. Mater.* **2017**, *27*, 1700493−1700501.
(109) Yin, C.; Zhen, X.; Fan, Q.; Huang, W.; Pu, K. Degradable Semiconducting Oligomer Amphiphile for Ratiometric Photoacoustic Imaging of Hypochlorite. *ACS Nano* **2017**, *11*, 4174−4182.
(110) Wu, L.; Wu, I. C.; DuFort, C. C.; Carlson, M. A.; Wu, X.; Chen, L.; Kuo, C.-T.; Qin, Y.; Yu, J.; Hingorani, S. R.; Chiu, D. T. Photostable Ratiometric Pdot Probe for In Vitro and In Vivo Imaging of Hypochlorous Acid. *J. Am. Chem. Soc.* **2017**, *139*, 6911−6918.
(111) Cone, C. J.; Bachyrycz, A. M.; Murata, G. H. Hepatotoxicity Associated with Metformin Therapy in Treatment of Type 2 Diabetes Mellitus with Nonalcoholic Fatty Liver Disease. *Ann. Pharmacother.* **2010**, *44*, 1655−1659.
(112) Malhotra, A.; Hepokoski, M.; McCowen, K. C.; Y-J Shyy, J. ACE2, Metformin, and COVID-19. *iScience* **2020**, *23*, 101425−101428.
(113) Chen, C. B.; Eurich, D. T.; Majumdar, S. R.; Johnson, J. A. Metformin and the Risk of Prostate Cancer across Racial/Ethnic Groups: A Population-Based Cohort Study. *Prostate Cancer Prostatic Dis.* **2017**, *20*, 122−126.
(114) Afshari, M. J.; Li, C.; Zeng, J.; Cui, J.; Wu, S.; Gao, M. Self-Illuminating NIR-II Bioluminescence Imaging Probe Based on Silver Sulfide Quantum Dots. *ACS Nano* **2022**, *16*, 16824−16832.
(115) Chen, W.; Zhang, Y.; Li, Q.; Jiang, Y.; Zhou, H.; Liu, Y.; Miao, Q.; Gao, M. Near-Infrared Afterglow Luminescence of Chlorin Nanoparticles for Ultrasensitive In Vivo Imaging. *J. Am. Chem. Soc.* **2022**, *144*, 6719−6726.
(116) Li, Q.; Zeng, J.; Miao, Q.; Gao, M. Self-Illuminating Agents for Deep-Tissue Optical Imaging. *Front. Bioeng. Biotechnol.* **2019**, *7*, 326−337.
(117) Lu, C.; Zhang, C.; Wang, P.; Zhao, Y.; Yang, Y.; Wang, Y.; Yuan, H.; Qu, S.; Zhang, X.; Song, G.; Pu, K. Light-Free Generation of Singlet Oxygen through Manganese-Thiophene Nanosystems for pH-Responsive Chemiluminescence Imaging and Tumor Therapy. *Chem.* **2020**, *6*, 2314−2334.
(118) Su, L.; Chen, Y.; Huo, H.; Liao, N.; Wu, Y.; Ge, X.; Guo, Z.; Chen, Z.; Zhang, X.; Song, J. NIR-II Ratiometric Chemiluminescent/Fluorescent Reporters for Real-Time Monitoring and Evaluating Cancer Photodynamic Therapy Efficacy. *Small* **2022**, *18*, 2202551−2202561.
(119) Ryan, L. S.; Gerberich, J.; Haris, U.; Nguyen, D.; Mason, R. P.; Lippert, A. R. Ratiometric pH Imaging Using a 1,2-Dioxetane Chemiluminescence Resonance Energy Transfer Sensor in Live Animals. *ACS Sens.* **2020**, *5*, 2925−2932.
(120) Liu, Y.; Teng, L.; Lyu, Y.; Song, G.; Zhang, X.-B.; Tan, W. Ratiometric Afterglow Luminescent Nanoplatform Enables Reliable Quantification and Molecular Imaging. *Nat. Commun.* **2022**, *13*, 2216−2228.
(121) Ong, T. T.; Ang, Z.; Verma, R.; Koean, R.; Tam, J. K. C.; Ding, J. L. pHLuc, a Ratiometric Luminescent Reporter for In Vivo Monitoring of Tumor Acidosis. *Front. Bioeng. Biotechnol.* **2020**, *8*, 412−422.
(122) Schlothauer, J. C.; Falckenhayn, J.; Perna, T.; Hackbarth, S.; Röder, B. Luminescence Investigation of Photosensitizer Distribution in Skin: Correlation of Singlet Oxygen Kinetics with the Microarchitecture of the Epidermis. *J. Biomed. Opt.* **2013**, *18*, 115001−115009.
(123) Murray, P. J. Macrophage Polarization. *Annu. Rev. Physiol.* **2017**, *79*, 541−566.
(124) Yao, Y.; Xu, X.-H.; Jin, L. Macrophage Polarization in Physiological and Pathological Pregnancy. *Front. Immunol.* **2019**, *10*, 792−804.
(125) DeNardo, D. G.; Ruffell, B. Macrophages as Regulators of Tumour Immunity and Immunotherapy. *Nat. Rev. Immunol.* **2019**, *19*, 369−382.
(126) Chen, Q.; Chen, M.; Liu, Z. Local Biomaterials-Assisted Cancer Immunotherapy to Trigger Systemic Antitumor Responses. *Chem. Soc. Rev.* **2019**, *48*, 5506−5526.
(127) Zhang, C.; Pu, K. Molecular and Nanoengineering Approaches Towards Activatable Cancer Immunotherapy. *Chem. Soc. Rev.* **2020**, *49*, 4234−4253.
(128) Badr, C. E. Bioluminescence Imaging: Basics and Practical Limitations. *Methods Mol. Biol.* **2014**, *1098*, 1−18.
(129) Syed, A. J.; Anderson, J. C. Applications of Bioluminescence in Biotechnology and Beyond. *Chem. Soc. Rev.* **2021**, *50*, 5668−5705.
(130) Lu, L.; Li, B.; Ding, S.; Fan, Y.; Wang, S.; Sun, C.; Zhao, M.; Zhao, C.-X.; Zhang, F. NIR-II Bioluminescence for In Vivo High Contrast Imaging and In Situ ATP-Mediated Metastases Tracing. *Nat. Commun.* **2020**, *11*, 4192−4202.
(131) Li, Q.; Ge, X.; Ye, J.; Li, Z.; Su, L.; Wu, Y.; Yang, H.; Song, J. Dual Ratiometric SERS and Photoacoustic Core-Satellite Nanoprobe for Quantitatively Visualizing Hydrogen Peroxide in Inflammation and Cancer. *Angew. Chem., Int. Ed.* **2021**, *60*, 7323−7332.
(132) Liu, X.; Gong, X.; Yuan, J.; Fan, X.; Zhang, X.; Ren, T.; Yang, S.; Yang, R.; Yuan, L.; Zhang, X.-B. Dual-Stimulus Responsive Near-Infrared Reversible Ratiometric Fluorescent and Photoacoustic Probe for In Vivo Tumor Imaging. *Anal. Chem.* **2021**, *93*, 5420−5429.
(133) Chen, Z.; Mu, X.; Han, Z.; Yang, S.; Zhang, C.; Guo, Z.; Bai, Y.; He, W. An Optical/Photoacoustic Dual-Modality Probe: Ratiometric In/Ex Vivo Imaging for Stimulated H_2S Upregulation in Mice. *J. Am. Chem. Soc.* **2019**, *141*, 17973−17977.
(134) Borek, C. Antioxidants and Radiation Therapy. *J. Nutr.* **2004**, *134*, 3207S−3209S.

https://doi.org/10.1021/acsnano.3c01641
ACS Nano XXXX, XXX, XXX−XXX

(135) Hassannia, B.; Vandenabeele, P.; Vanden Berghe, T. Targeting Ferroptosis to Iron out Cancer. *Cancer Cell* **2019**, *35*, 830−849.
(136) Wu, L.; Ishigaki, Y.; Zeng, W.; Harimoto, T.; Yin, B.; Chen, Y.; Liao, S.; Liu, Y.; Sun, Y.; Zhang, X.; Liu, Y.; Liang, Y.; Sun, P.; Suzuki, T.; Song, G.; Fan, Q.; Ye, D. Generation of Hydroxyl Radical-Activatable Ratiometric Near-Infrared Bimodal Probes for Early Monitoring of Tumor Response to Therapy. *Nat. Commun.* **2021**, *12*, 6145−6157.
(137) Zhao, X.; Ji, H.; Hasrat, K.; Misal, S.; He, F.; Dai, Y.; Ma, F.; Qi, Z. A Mitochondria-Targeted Single Fluorescence Probe for Separately and Continuously Visualizing H_2S and Cys with Multi-Response Signals. *Anal. Chim. Acta* **2020**, *1107*, 172−182.
(138) Zhao, F.; Zhai, Z.; Tang, J.; Zhang, B.; Yang, X.; Song, X.; Ye, Y. A Bond Energy Transfer Based Difunctional Fluorescent Sensor for Cys and Bisulfite. *Talanta* **2020**, *214*, 120884−120891.
(139) Ai, X.; Wang, Z.; Cheong, H.; Wang, Y.; Zhang, R.; Lin, J.; Zheng, Y.; Gao, M.; Xing, B. Multispectral Optoacoustic Imaging of Dynamic Redox Correlation and Pathophysiological Progression Utilizing Upconversion Nanoprobes. *Nat. Commun.* **2019**, *10*, 1087−1097.
(140) Wang, H.; Wang, W.; Liu, L.; Wang, M.; Li, G.; Li, H.; Li, B.; Yu, S.; Ma, D.; Xue, W. Biodegradable Hollow Polydopamine@ Manganese Dioxide as an Oxygen Self-Supplied Nanoplatform for Boosting Chemo-Photodynamic Cancer Therapy. *ACS Appl. Mater. Interfaces* **2021**, *13*, 57009−57022.
(141) Wang, S.; Wang, Z.; Yu, G.; Zhou, Z.; Jacobson, O.; Liu, Y.; Ma, Y.; Zhang, F.; Chen, Z.-Y.; Chen, X. Tumor-Specific Drug Release and Reactive Oxygen Species Generation for Cancer Chemo/Chemodynamic Combination Therapy. *Adv. Sci.* **2019**, *6*, 1801986−1801992.
(142) Liu, Y.; Jia, Q.; Guo, Q.; Wei, W.; Zhou, J. Simultaneously Activating Highly Selective Ratiometric MRI and Synergistic Therapy in Response to Intratumoral Oxidability and Acidity. *Biomaterials* **2018**, *180*, 104−116.
(143) Hou, Y.; Zhou, J.; Gao, Z.; Sun, X.; Liu, C.; Shangguan, D.; Yang, W.; Gao, M. Protease-Activated Ratiometric Fluorescent Probe for pH Mapping of Malignant Tumors. *ACS Nano* **2015**, *9*, 3199−3205.
(144) Zhang, Q.; Zhu, Z.; Zheng, Y.; Cheng, J.; Zhang, N.; Long, Y.-T.; Zheng, J.; Qian, X.; Yang, Y. A Three-Channel Fluorescent Probe That Distinguishes Peroxynitrite from Hypochlorite. *J. Am. Chem. Soc.* **2012**, *134*, 18479−18482.
(145) Huang, T.; Yan, S.; Yu, Y.; Xue, Y.; Yu, Y.; Han, C. Dual-Responsive Ratiometric Fluorescent Probe for Hypochlorite and Peroxynitrite Detection and Imaging In Vitro and In Vivo. *Anal. Chem.* **2022**, *94*, 1415−1424.
(146) Sharma, N.; Yun, K. Dual Sensing of Tetracycline and L-Lysine Using Green Synthesized Carbon Dots from Nigella Sativa Seeds. *Dyes Pigm.* **2020**, *182*, 108640−108648.
(147) Gao, P.; Xie, Z.; Zheng, M. Chiral Carbon Dots-Based Nanosensors for Sn(II) Detection and Lysine Enantiomers Recognition. *Sens. Actuators, B* **2020**, *319*, 128265−128272.
(148) Jiang, X.-D.; Yue, S.; Jia, L.; Li, S.; Li, C.; Li, Q.; Xiao, L. NIR Fluorescent Azabodipy-Based Probe for the Specific Detection of L-Lysine. *ChemistrySelect* **2018**, *3*, 7581−7585.
(149) Chang, D.; Zhao, Z.; Shi, H.; Feng, J.; Yang, Y.; Shi, L. Ratiometric Fluorescent Carbon Dots for Enantioselective Sensing of L-Lysine and pH Discrimination In Vivo and In Vitro. *Sens. Actuators, B* **2022**, *362*, 131792−131796.
(150) Aoyama, K.; Nakaki, T. Glutathione in Cellular Redox Homeostasis: Association with the Excitatory Amino Acid Carrier 1 (EAAC1). *Molecules* **2015**, *20*, 8742−8758.
(151) Wu, L.; Zeng, W.; Ishigaki, Y.; Zhang, J.; Bai, H.; Harimoto, T.; Suzuki, T.; Ye, D. A Ratiometric Photoacoustic Probe with a Reversible Response to Hydrogen Sulfide and Hydroxyl Radicals for Dynamic Imaging of Liver Inflammation. *Angew. Chem., Int. Ed.* **2022**, *61*, 202209248−202209255.
(152) Wang, M.; Liu, Q.; Sun, X.; Zheng, S.; Ma, Y.; Wang, Y.; Yan, M.; Lu, Z.; Fan, C.; Lin, W. Ratiometric and Reversible Detection of Endogenous SO_2 and HCHO in Living Cells and Mice by a Near-Infrared and Dual-Emission Fluorescent Probe. *Sens. Actuators, B* **2021**, *335*, 129649−129657.
(153) Zheng, J.; Zeng, Q.; Zhang, R.; Xing, D.; Zhang, T. Dynamic-Reversible Photoacoustic Probe for Continuous Ratiometric Sensing and Imaging of Redox Status In Vivo. *J. Am. Chem. Soc.* **2019**, *141*, 19226−19230.
(154) Zhang, C.; Gao, R.; Zhang, L.; Liu, C.; Yang, Z.; Zhao, S. Design and Synthesis of a Ratiometric Photoacoustic Probe for In Situ Imaging of Zinc Ions in Deep Tissue In Vivo. *Anal. Chem.* **2020**, *92*, 6382−6390.
(155) Ma, Y.; Gao, W.; Zhu, L.; Zhao, Y.; Lin, W. A Ratiometric Fluorescent Probe for Reversible Monitoring of Endogenous SO_2/Formaldehyde in Cytoplasm and Nucleoli Regions and Its Applications in Living Mice. *Analyst* **2020**, *145*, 1865−1870.
(156) Ma, J.; Li, F.; Li, Q.; Li, Y.; Yan, C.; Lu, X.; Guo, Y. Naked-Eye and Ratiometric Fluorescence Probe for Fast and Sensitive Detection of Hydrogen Sulfide and Its Application in Bioimaging. *New J. Chem.* **2018**, *42*, 19272−19278.
(157) Wan, S.; Xia, S.; Medford, J.; Durocher, E.; Steenwinkel, T. E.; Rule, L.; Zhang, Y.; Luck, R. L.; Werner, T.; Liu, H. A Ratiometric near-Infrared Fluorescent Probe Based on a Novel Reactive Cyanine Platform for Mitochondrial pH Detection. *J. Mater. Chem. B* **2021**, *9*, 5150−5161.
(158) Szabo, C. Gasotransmitters in Cancer: From Pathophysiology to Experimental Therapy. *Nat. Rev. Drug Discovery* **2016**, *15*, 185−203.
(159) Wu, Q.; Yin, C.; Wen, Y.; Zhang, Y.; Huo, F. An ICT Lighten Ratiometric and NIR Fluorogenic Probe to Visualize Endogenous/Exogenous Hydrogen Sulphide and Imaging in Mice. *Sens. Actuators, B* **2019**, *288*, 507−511.
(160) Yang, B.; Chen, Y.; Shi, J. Reactive Oxygen Species (ROS)-Based Nanomedicine. *Chem. Rev.* **2019**, *119*, 4881−4985.
(161) Ezeriņa, D.; Takano, Y.; Hanaoka, K.; Urano, Y.; Dick, T. P. N-Acetyl Cysteine Functions as a Fast-Acting Antioxidant by Triggering Intracellular H_2S and Sulfane Sulfur Production. *Cell Chem. Biol.* **2018**, *25*, 447−459.e4.
(162) Wu, L.; Zeng, W.; Feng, L.; Hu, Y.; Sun, Y.; Yan, Y.; Chen, H.-Y.; Ye, D. An Activatable Ratiometric Near-Infrared Fluorescent Probe for Hydrogen Sulfide Imaging In Vivo. *Sci. China Chem.* **2020**, *63*, 741−750.
(163) Yang, S.; Lian, G. Ros and Diseases: Role in Metabolism and Energy Supply. *Mol. Cell. Biochem.* **2020**, *467*, 1−12.
(164) Wang, Q.; Ding, X.; Wang, Y.; Du, Q.; Xu, T.; Du, B.; Yao, H. The Ratiometric Fluorescence Nanoparticle Based on SiRB for pH Detection of Tumor. *Eur. J. Pharm. Sci.* **2018**, *118*, 32−39.
(165) Zhang, Y.; Xia, S.; Mikesell, L.; Whisman, N.; Fang, M.; Steenwinkel, T. E.; Chen, K.; Luck, R. L.; Werner, T.; Liu, H. Near-Infrared Hybrid Rhodol Dyes with Spiropyran Switches for Sensitive Ratiometric Sensing of pH Changes in Mitochondria and Drosophila Melanogaster First-Instar Larvae. *ACS Appl. Bio Mater.* **2019**, *2*, 4986−4997.
(166) Xia, S.; Wang, J.; Zhang, Y.; Whisman, N.; Bi, J.; Steenwinkel, T. E.; Wan, S.; Medford, J.; Tajiri, M.; Luck, R. L.; Werner, T.; Liu, H. Ratiometric Fluorescent Probes Based on Through-Bond Energy Transfer of Cyanine Donors to Near-Infrared Hemicyanine Acceptors for Mitochondrial pH Detection and Monitoring of Mitophagy. *J. Mater. Chem. B* **2020**, *8*, 1603−1615.
(167) Chen, H.; Ding, F.; Zhou, Z.; He, X.; Shen, J. FRET-Based Sensor for Visualizing pH Variation with Colorimetric/Ratiometric Strategy and Application for Bioimaging in Living Cells, Bacteria and Zebrafish. *Analyst* **2020**, *145*, 4283−4294.
(168) Shi, L.; Yan, C.; Guo, Z.; Chi, W.; Wei, J.; Liu, W.; Liu, X.; Tian, H.; Zhu, W.-H. De Novo Strategy with Engineering Anti-Kasha/Kasha Fluorophores Enables Reliable Ratiometric Quantification of Biomolecules. *Nat. Commun.* **2020**, *11*, 793−803.
(169) Niu, W.; Jia, J.; Li, J.; Zhang, C.; Yun, K. Ratiometric Emission NIR-Fluorescent Probe for the Detection of Lysosomal pH in Living Cells and In Vivo. *New J. Chem.* **2019**, *43*, 13363−13370.

https://doi.org/10.1021/acsnano.3c01641
ACS Nano XXXX, XXX, XXX−XXX

(170) Shu, W.; Yu, J.; Li, Z.; Sun, X.; Wang, Y.; Wu, Y.; Qin, J.; Zhang, Y.; Xiao, H.; Zhang, X. A Mitochondrial Suitable Ratiometric Fluorescent Probe for Tracking pH Change During Mitophagy. *Sens. Actuators, B* **2022**, *369*, 132323−132329.
(171) Chen, H.; Luo, J.; Chen, S.; Qi, Y.; Zhou, T.; Tian, X.; Ding, F. Sensing Hypochlorite or pH Variations in Live Cells and Zebrafish with a Novel Dual-Functional Ratiometric and Colorimetric Chemosensor. *Spectrochim. Acta, Part A* **2022**, *271*, 120915−120924.
(172) Bilal, M.; Cui, J.; Iqbal, H. M. N. Tailoring Enzyme Microenvironment: State-of-the-Art Strategy to Fulfill the Quest for Efficient Bio-Catalysis. *Int. J. Biol. Macromol.* **2019**, *130*, 186−196.
(173) Boron, W. F. Regulation of Intracellular pH. *Adv. Physiol. Educ.* **2004**, *28*, 160−179.
(174) Fan, H.; Yan, G.; Zhao, Z.; Hu, X.; Zhang, W.; Liu, H.; Fu, X.; Fu, T.; Zhang, X.-B.; Tan, W. A Smart Photosensitizer-Manganese Dioxide Nanosystem for Enhanced Photodynamic Therapy by Reducing Glutathione Levels in Cancer Cells. *Angew. Chem., Int. Ed.* **2016**, *55*, 5477−5482.
(175) Liu, F.; Lin, L.; Zhang, Y.; Wang, Y.; Sheng, S.; Xu, C.; Tian, H.; Chen, X. A Tumor-Microenvironment-Activated Nanozyme-Mediated Theranostic Nanoreactor for Imaging-Guided Combined Tumor Therapy. *Adv. Mater.* **2019**, *31*, 1902885−1902895.
(176) Muri, J.; Kopf, M. Redox Regulation of Immunometabolism. *Nat. Rev. Immunol.* **2021**, *21*, 363−381.
(177) Gurtner, G. C.; Werner, S.; Barrandon, Y.; Longaker, M. T. Wound Repair and Regeneration. *Nature* **2008**, *453*, 314−321.
(178) Boxhoorn, L.; Voermans, R. P.; Bouwense, S. A.; Bruno, M. J.; Verdonk, R. C.; Boermeester, M. A.; van Santvoort, H. C.; Besselink, M. G. Acute Pancreatitis. *Lancet* **2020**, *396*, 726−734.
(179) Johnston, D. E. Special Considerations in Interpreting Liver Function Tests. *Am. Fam. Physician* **1999**, *59*, 2223−2230.
(180) Li, X.; Liu, Y.; Qi, X.; Xiao, S.; Xu, Z.; Yuan, Z.; Liu, Q.; Li, H.; Ma, S.; Liu, T.; Huang, Y.; Zhang, X.; Zhang, X.; Mao, Z.; Luo, G.; Deng, J. Sensitive Activatable Nanoprobes for Real-Time Ratiometric Magnetic Resonance Imaging of Reactive Oxygen Species and Ameliorating Inflammation In Vivo. *Adv. Mater.* **2022**, *34*, 2109004−2109017.
(181) Zhang, P.; Zeng, J.; Li, Y.; Yang, C.; Meng, J.; Hou, Y.; Gao, M. Quantitative Mapping of Glutathione within Intracranial Tumors through Interlocked MRI Signals of a Responsive Nanoprobe. *Angew. Chem., Int. Ed.* **2021**, *60*, 8130−8138.
(182) Gao, Z.; Hou, Y.; Zeng, J.; Chen, L.; Liu, C.; Yang, W.; Gao, M. Tumor Microenvironment-Triggered Aggregation of Antiphagocytosis ^{99m}Tc-Labeled Fe_3O_4 Nanoprobes for Enhanced Tumor Imaging In Vivo. *Adv. Mater.* **2017**, *29*, 1701095−1701101.
(183) Tang, Q.; Cao, S.; Ma, T.; Xiang, X.; Luo, H.; Borovskikh, P.; Rodriguez, R. D.; Guo, Q.; Qiu, L.; Cheng, C. Engineering Biofunctional Enzyme-Mimics for Catalytic Therapeutics and Diagnostics. *Adv. Funct. Mater.* **2021**, *31*, 2007475−2007503.
(184) Yin, C.; Tang, Y.; Li, X.; Yang, Z.; Li, J.; Li, X.; Huang, W.; Fan, Q. A Single Composition Architecture-Based Nanoprobe for Ratiometric Photoacoustic Imaging of Glutathione (GSH) in Living Mice. *Small* **2018**, *14*, 1703400−1703406.
(185) Yoshihara, T.; Hirakawa, Y.; Hosaka, M.; Nangaku, M.; Tobita, S. Oxygen Imaging of Living Cells and Tissues Using Luminescent Molecular Probes. *J. Photochem. Photobiol., C* **2017**, *30*, 71−95.
(186) Wang, S.; Gu, K.; Guo, Z.; Yan, C.; Yang, T.; Chen, Z.; Tian, H.; Zhu, W.-H. Self-Assembly of a Monochromophore-Based Polymer Enables Unprecedented Ratiometric Tracing of Hypoxia. *Adv. Mater.* **2019**, *31*, 1805735−1805741.
(187) Xiao, P.; Liu, C.; Ma, T.; Lu, X.; Jing, L.; Hou, Y.; Zhang, P.; Huang, G.; Gao, M. A Cyclodextrin-Hosted Ir(III) Complex for Ratiometric Mapping of Tumor Hypoxia In Vivo. *Adv. Sci.* **2021**, *8*, 2004044−2004054.
(188) Jiang, G.; Li, C.; Lai, Q.; Liu, X.; Chen, Q.; Zhang, P.; Wang, J.; Tang, B. Z. An Easily Available Ratiometric AIE Probe for Peroxynitrite In Vitro and In Vivo Imaging. *Sens. Actuators, B* **2021**, *329*, 129223−129229.
(189) Gu, B.; Liu, M.; Dai, C.; Zhou, Z.; Tang, D.; Tang, S.; Shen, Y.; Li, H. Rational Construction of a Novel Ratiometric Far-Red Fluorescent Probe with Excellent Water Solubility for Sensing Mitochondrial Peroxynitrite. *Sens. Actuators, B* **2021**, *344*, 130246−130254.
(190) Wang, J.; Liu, L.; Xu, W.; Yang, Z.; Yan, Y.; Xie, X.; Wang, Y.; Yi, T.; Wang, C.; Hua, J. Mitochondria-Targeted Ratiometric Fluorescent Probe Based on Diketopyrrolopyrrole for Detecting and Imaging of Endogenous Superoxide Anion In Vitro and In Vivo. *Anal. Chem.* **2019**, *91*, 5786−5793.
(191) Taverne, Y. J.; Bogers, A. J.; Duncker, D. J.; Merkus, D. Reactive Oxygen Species and the Cardiovascular System. *Oxid. Med. Cell. Longev.* **2013**, *2013*, 862423.
(192) Hall, C. N.; Garthwaite, J. What Is the Real Physiological NO Concentration In Vivo? *Nitric Oxide* **2009**, *21*, 92−103.
(193) Sharma, A.; Sharma, N.; Sharma, N.; Sharma, R. K.; Gupta, A. K. Recent Advances in Biomedical Imaging: A Review. *J. Med. Eng. Technol.* **2021**, *45*, 277−293.

https://doi.org/10.1021/acsnano.3c01641
ACS Nano XXXX, XXX, XXX−XXX